

INFORMATION TO USERS

This reproduction was made from a copy of a document sent to us for microfilming. While the most advanced technology has been used to photograph and reproduce this document, the quality of the reproduction is heavily dependent upon the quality of the material submitted.

The following explanation of techniques is provided to help clarify markings or notations which may appear on this reproduction.

1. The sign or "target" for pages apparently lacking from the document photographed is "Missing Page(s)". If it was possible to obtain the missing page(s) or section, they are spliced into the film along with adjacent pages. This may have necessitated cutting through an image and duplicating adjacent pages to assure complete continuity.
2. When an image on the film is obliterated with a round black mark, it is an indication of either blurred copy because of movement during exposure, duplicate copy, or copyrighted materials that should not have been filmed. For blurred pages, a good image of the page can be found in the adjacent frame. If copyrighted materials were deleted, a target note will appear listing the pages in the adjacent frame.
3. When a map, drawing or chart, etc., is part of the material being photographed, a definite method of "sectioning" the material has been followed. It is customary to begin filming at the upper left hand corner of a large sheet and to continue from left to right in equal sections with small overlaps. If necessary, sectioning is continued again--beginning below the first row and continuing on until complete.
4. For illustrations that cannot be satisfactorily reproduced by xerographic means, photographic prints can be purchased at additional cost and inserted into your xerographic copy. These prints are available upon request from the Dissertations Customer Services Department.
5. Some pages in any document may have indistinct print. In all cases the best available copy has been filmed.

**University
Microfilms
International**
300 N. Zeeb Road
Ann Arbor, MI 48106

1323208

MARINELLI, FREDERICK

ANALYSIS OF CONSTANT HEAD INJECTION TESTS IN SINGLE,
PARTIALLY PENETRATING BOREHOLES

THE UNIVERSITY OF ARIZONA

M.S. 1984

**University
Microfilms
International** 300 N. Zeeb Road, Ann Arbor, MI 48106

Copyright 1984

by

MARINELLI, FREDERICK
All Rights Reserved

PLEASE NOTE:

In all cases this material has been filmed in the best possible way from the available copy. Problems encountered with this document have been identified here with a check mark .

1. Glossy photographs or pages _____
2. Colored illustrations, paper or print _____
3. Photographs with dark background _____
4. Illustrations are poor copy _____
5. Pages with black marks, not original copy _____
6. Print shows through as there is text on both sides of page _____
7. Indistinct, broken or small print on several pages
8. Print exceeds margin requirements _____
9. Tightly bound copy with print lost in spine _____
10. Computer printout pages with indistinct print _____
11. Page(s) _____ lacking when material received, and not available from school or author.
12. Page(s) _____ seem to be missing in numbering only as text follows.
13. Two pages numbered _____. Text follows.
14. Curling and wrinkled pages _____
15. Other _____

University
Microfilms
International

ANALYSIS OF CONSTANT HEAD INJECTION TESTS IN
SINGLE, PARTIALLY PENETRATING BOREHOLES

by

Frederick Marinelli

A Thesis Submitted to the Faculty of the
DEPARTMENT OF HYDROLOGY AND WATER RESOURCES
In Partial Fulfillment of the Requirements
for the Degree of

MASTER OF SCIENCE
WITH A MAJOR IN HYDROLOGY

In the Graduate College
THE UNIVERSITY OF ARIZONA

1 9 8 4

Copyright 1984 Frederick Marinelli

STATEMENT BY AUTHOR

This thesis has been submitted in partial fulfillment of requirements for an advanced degree at The University of Arizona and is deposited in the University Library to be made available to borrowers under rules of the Library.

Brief quotations from this thesis are allowable without special permission, provided that accurate acknowledgement of source is made. Requests for permission for extended quotation from or reproduction of this manuscript in whole or in part may be granted by the copyright holder.

SIGNED: Frederick Marinelli

APPROVAL BY THESIS DIRECTOR

This thesis has been approved on the date shown below:

S. P. Neuman
S.P. Neuman
Professor of Hydrology

10/12/1983
Date

TABLE OF CONTENTS

	Page
LIST OF ILLUSTRATIONS	iv
LIST OF TABLES	vi
ABSTRACT	vii
1. INTRODUCTION	1
2. MATHEMATICAL STATEMENT OF THE PROBLEM	5
3. NUMERICAL ANALYSIS	12
3.1 Mesh Analysis	14
3.2 Transient Horizontal Flow	16
3.3 Transient Nonhorizontal Flow	21
3.4 Curve Matching Procedure for Determination of Hydraulic Conductivity	27
4. STEADY-STATE ANALYSIS	32
4.1 Comparison with Numerical Results	39
4.2 Multiple Rate Testing	44
4.3 Error Analysis	48
5. CONCLUSIONS	51
APPENDIX: NOMENCLATURE	54
LIST OF REFERENCES	57

LIST OF ILLUSTRATIONS

Figure		Page
1.	Typical Piezometer and Packer Installations	2
2.	Flow Field in the Vicinity of a Partially Penetrating Borehole	6
3.	Horizontal Flow From a Borehole	9
4.	Type Curve (Q_D vs. t_D) for Strictly Horizontal Flow	11
5.	Boundary Conditions for Numerical Simulation of Strictly Horizontal Flow	17
6.	Comparison of Numerical Results with Exact Solution for Strictly Horizontal Flow	20
7.	Boundary Conditions for Numerical Simulation of Nonhorizontal Flow ($\gamma = 5$)	22
8.	Comparison of Numerical Results from MESH-5A, MESH-5B, and MESH-5C	26
9.	Type Curves (Q_D vs. t_D) for Transient Nonhorizontal Flow	29
10.	Line Source Approximation	35
11.	Cylindrical Borehole Approximated with Prolate Spheroid	37
12.	Comparison of Numerical Shape Factor with Analytical Approximations	40
13.	Steady-State Hydraulic Buildup Distribution Predicted by Approximation 3 ($\gamma = 10$)	42
14.	Steady-State Hydraulic Buildup Distribution Predicted by Numerical Results ($\gamma = 10$)	43
15.	Distribution of Flux Along the Borehole	45
16.	Multiple Rate Tests	46

LIST OF ILLUSTRATIONS--Continued

Plate

- | | | |
|----|--|-----------|
| 1. | Exterior Mesh and Interior Meshes for Strictly Horizontal Flow | In pocket |
| 2. | Exterior Mesh and Interior Meshes for Nonhorizontal Flow ($\gamma = 5$) | In pocket |
| 3. | Full Size Type Curves (Q_D vs. t_D) for Transient Nonhorizontal Flow | In pocket |

LIST OF TABLES

Table		Page
1.	Performance of FLUMPS in Simulating Strictly Horizontal Flow	19
2.	Performance of FLUMPS in Simulating Nonhorizontal Flow ($\gamma = 5$)	25
3.	Performance of FLUMPS for Each "A" Mesh	28

ABSTRACT

The flow rate from a piezometer or packer installation, in which a constant pressure head is maintained, is examined analytically and numerically. The partially penetrating borehole is assumed to have finite dimensions and is situated in a homogeneous anisotropic medium of infinite thickness and radial extent. For the general case of transient nonhorizontal flow, the problem is solved numerically by modeling the flow system with finite elements. A curve matching procedure for determining horizontal and vertical hydraulic conductivity is investigated. The method has several limitations because the resulting type curves have similar shapes for conditions of practical interest. It is concluded that a reliable determination of vertical hydraulic conductivity cannot be made from single borehole tests. The numerical solution is used to evaluate existing steady-state analytical approximations. An empirical "shape factor" equation, obtained from the numerical results, is presented as an improvement to that given by Hvorslev (1951).

CHAPTER 1

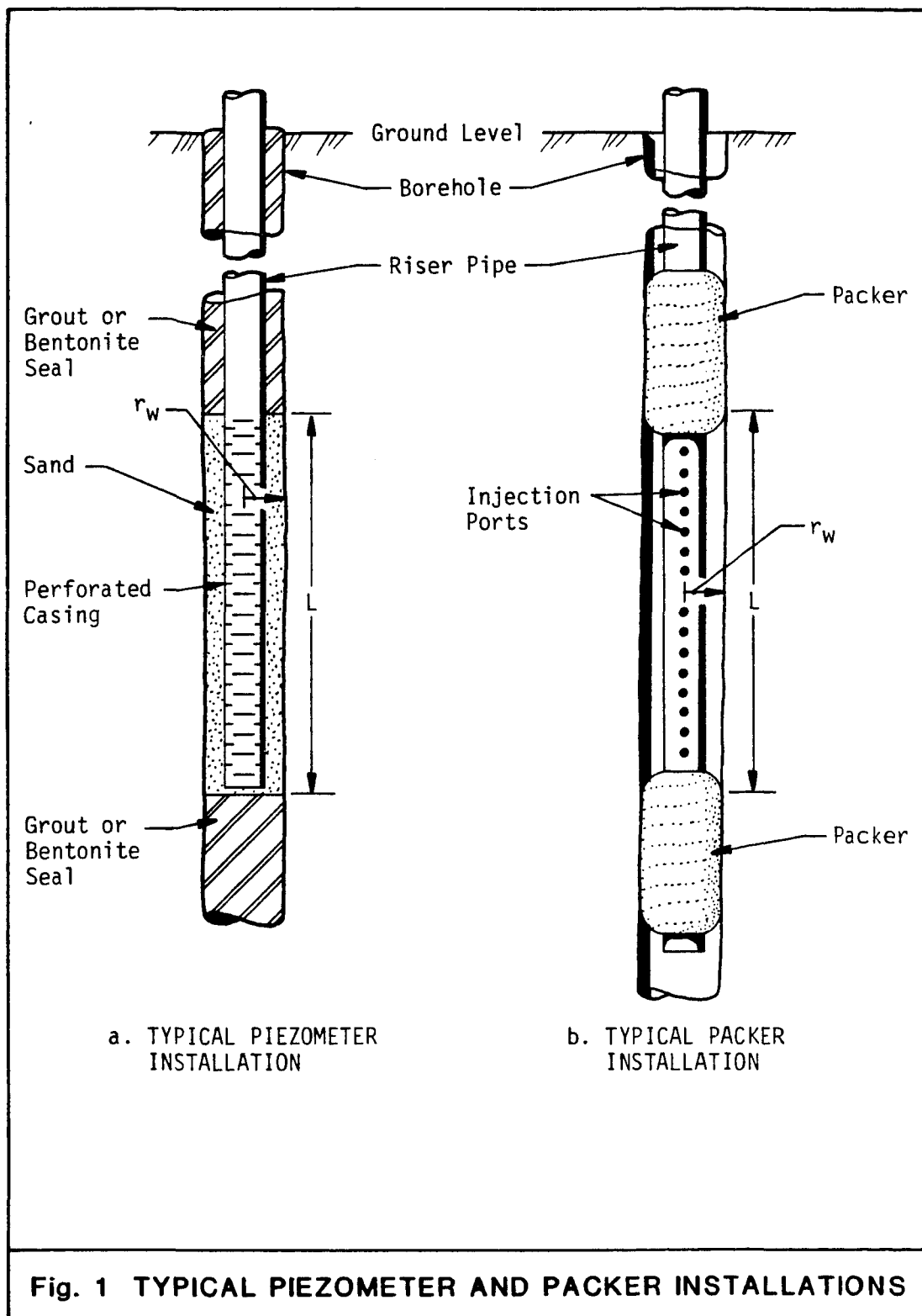
INTRODUCTION

Hydrologists often rely on constant flow rate pump tests in single boreholes for in situ determination of hydraulic conductivity. However, under certain field conditions, the constant flow rate test may not be feasible. For example:

- In geologic materials of low permeability, it may be difficult to maintain constant flow rates over time due to excessive pumping pressures (injection tests) or dewatering of the borehole (withdrawal tests).
- Constant flow rate withdrawal tests require the installation of a pump in the borehole. A pump installation may not be feasible in small diameter casings.
- The equipment required for constant flow rate injection may be more costly than that of other methods.
- Constant flow rate withdrawal tests may not be practical when low piezometric heads result in excessive pumping lifts.

In situations where constant flow rate tests are not easily performed, it is commonly more practical to perform a pump test where a constant pressure head is maintained in the borehole and flow rate is measured as a function of time.

Figure 1a shows a typical piezometer installation in which the tested portion of a borehole is isolated by means of a permanent grout



or bentonite seal. Figure 1b illustrates a packer installation which temporarily isolates a section of an open borehole by means of pneumatic or mechanical seals. Hydrologists generally use the same mathematical techniques for analyzing hydrological tests conducted in both types of installations. Since the analytical and numerical solutions in this paper conform more closely to piezometer installations, the descriptions which follow will place secondary importance on packer installations.

Jacob and Lohman (1952) presented a closed form analytical solution for the special case of transient, strictly horizontal flow, from a borehole of finite radius. Their solution was based on the work of Smith (1937) for the analogous heat flow problem. A similar solution (yielding the same numerical values) was given by Van Everdingen and Hurst (1949). Strictly horizontal flow may be a reasonable assumption for any of the following field conditions:

- The tested portion of the borehole fully penetrates a stratum of constant thickness which is bounded above and below by materials of much lower permeability.
- The medium is strongly anisotropic with horizontal permeability much greater than that in the vertical direction.
- The length of the tested portion of the borehole is very large compared to its diameter.

The assumption of strictly horizontal flow is of questionable validity in situations where none of these conditions is satisfied.

Hvorslev (1951) presented a series of steady-state equations for the more general case of nonhorizontal flow to a partially

penetrating borehole. His equations disregard medium storage and are based on dimensionless "shape factors" which depend on the geometry of the tested portion of the borehole and the anisotropy of the medium. Hvorslev does not show how his equations are derived, nor does he specifically state all the assumptions utilized. It is therefore difficult to judge the validity of Hvorslev's method from his work alone. Furthermore, many of the references cited in his paper are not readily available.

An apparent contradiction exists between Hvorslev's steady-state equations and the Jacob-Lohman solution (which indicates that the system never achieves steady-state). However, constant head field tests commonly seem to reach steady-state conditions after an initial transient period.

The purpose of this study is to extend the Jacob-Lohman solution for the more general case of transient nonhorizontal flow from a partially penetrating borehole in a medium of infinite thickness and radial extent. The problem is solved numerically using a saturated flow, finite element model. Based on the numerical results, a method is proposed for determining hydraulic conductivity from constant head tests performed in partially penetrating boreholes. After the transient solution is obtained, Hvorslev's steady-state approach is evaluated and an improved shape factor equation is proposed.

CHAPTER 2

MATHEMATICAL STATEMENT OF THE PROBLEM

For a homogeneous anisotropic medium of infinite thickness and radial extent, the flow field about a piezometer installation, in which a constant head is maintained, is stated mathematically by the following set of equations (refer to Figure 2):

$$K_r \left(\frac{\partial^2 s}{\partial r^2} + \frac{1}{r} \frac{\partial s}{\partial r} \right) + K_z \frac{\partial^2 s}{\partial z^2} = S_s \frac{\partial s}{\partial t}$$

$$r > r_w; -\infty < z < \infty; t > 0 \quad (2-1)$$

$$s(r, z, 0) = 0 \quad (2-2)$$

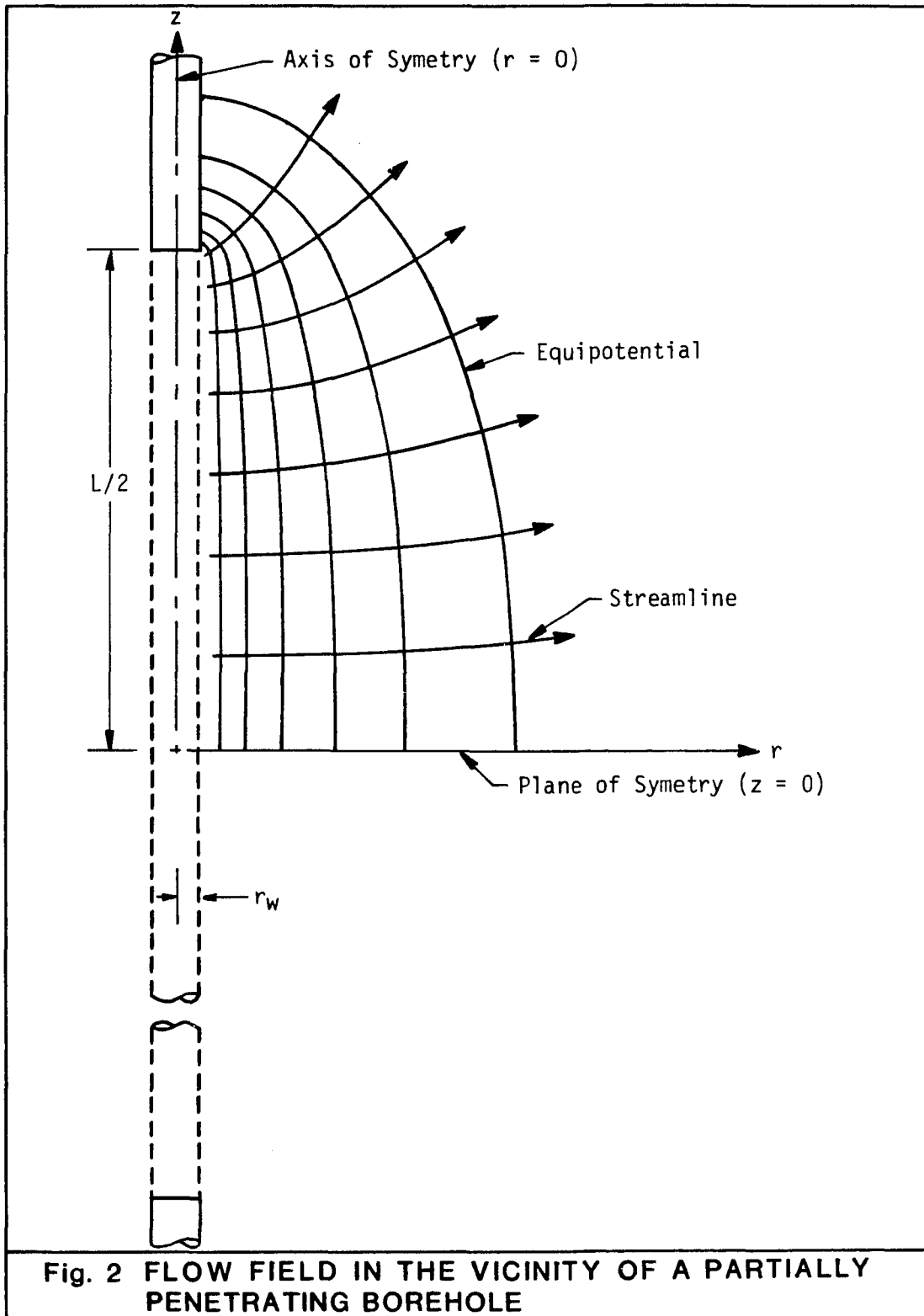
$$s(\infty, z, t) = 0 \quad (2-3)$$

$$s(r, \pm \infty, t) = 0 \quad (2-4)$$

$$s(r_w, z, t) = s_0 \quad -\frac{L}{2} \leq z \leq \frac{L}{2} \quad (2-5)$$

$$\frac{\partial s}{\partial r} \Big|_{r_w} = 0 \quad z < -\frac{L}{2}; z > \frac{L}{2} \quad (2-6)$$

where s is the hydraulic buildup (or drawdown), S_s the specific storage, r_w the borehole radius, L the length of the tested portion of the borehole, and K_r and K_z are the principal hydraulic conductivities which have directions parallel to the r and z coordinate axes respectively. Boundary conditions (2-3) and (2-4) imply that the change in head is zero at an infinite distance from the piezometer. Boundary condition (2-5) prescribes a constant hydraulic buildup (s_0) along the



open portion of the borehole and (2-6) specifies a no-flow boundary elsewhere along the borehole radius.

The piezometer flow rate (Q) is determined by applying Darcy's law at the borehole radius and integrating along the open portion of the borehole.

$$Q(t) = - 2\pi r_w K_r \int_{-\frac{L}{2}}^{\frac{L}{2}} \frac{\partial \Delta}{\partial r}(r_w, z, t) dz \quad (2-7)$$

By making the following substitutions in (2-1),

$$m = \sqrt{\frac{K_r}{K_z}} \quad (2-8)$$

$$R = \frac{r}{m} \quad (2-9)$$

$$S_s^* = m^2 S_s \quad (2-10)$$

the anisotropic flow equation simplifies to,

$$\frac{\partial^2 \Delta}{\partial R^2} + \frac{1}{R} \frac{\partial \Delta}{\partial R} + \frac{\partial^2 \Delta}{\partial z^2} = \frac{S_s^*}{K_r} \frac{\partial \Delta}{\partial t} \quad (2-11)$$

which is simply the isotropic case in an (R, z) coordinate system.

Thus, an anisotropic flow system can be simulated by first determining the flow field in an "equivalent isotropic medium" of the (R, z) coordinate system with hydraulic conductivity equal to K_r and specific storage equal to S_s^* , and then transforming the radial coordinates using equation (2-9). We therefore wish to solve equation (2-11) subject to the following conditions:

$$\delta(R, z, 0) = 0 \quad (2-12)$$

$$\delta(\infty, z, t) = 0 \quad (2-13)$$

$$\delta(R, \pm \infty, t) = 0 \quad (2-14)$$

$$\delta(R_w, z, t) = \delta_0 \quad -\frac{L}{2} \leq z \leq \frac{L}{2} \quad (2-15)$$

$$\left. \frac{\partial \delta}{\partial R} \right|_{R_w} = 0 \quad z < -\frac{L}{2}; z > \frac{L}{2} \quad (2-16)$$

A closed-form solution is not available for the mathematical problem defined by equations (2-11) through (2-16).

For the special case of transient, strictly horizontal flow in a homogeneous medium of infinite radial extent, the mathematical problem is given by the following set of equations (refer to Figure 3):

$$\frac{\partial^2 \delta}{\partial r^2} + \frac{1}{r} \frac{\partial \delta}{\partial r} = \frac{S_s}{K_r} \frac{\partial \delta}{\partial t} \quad r > r_w; t > 0 \quad (2-17)$$

$$\delta(r, 0) = 0 \quad (2-18)$$

$$\delta(\infty, t) = 0 \quad (2-19)$$

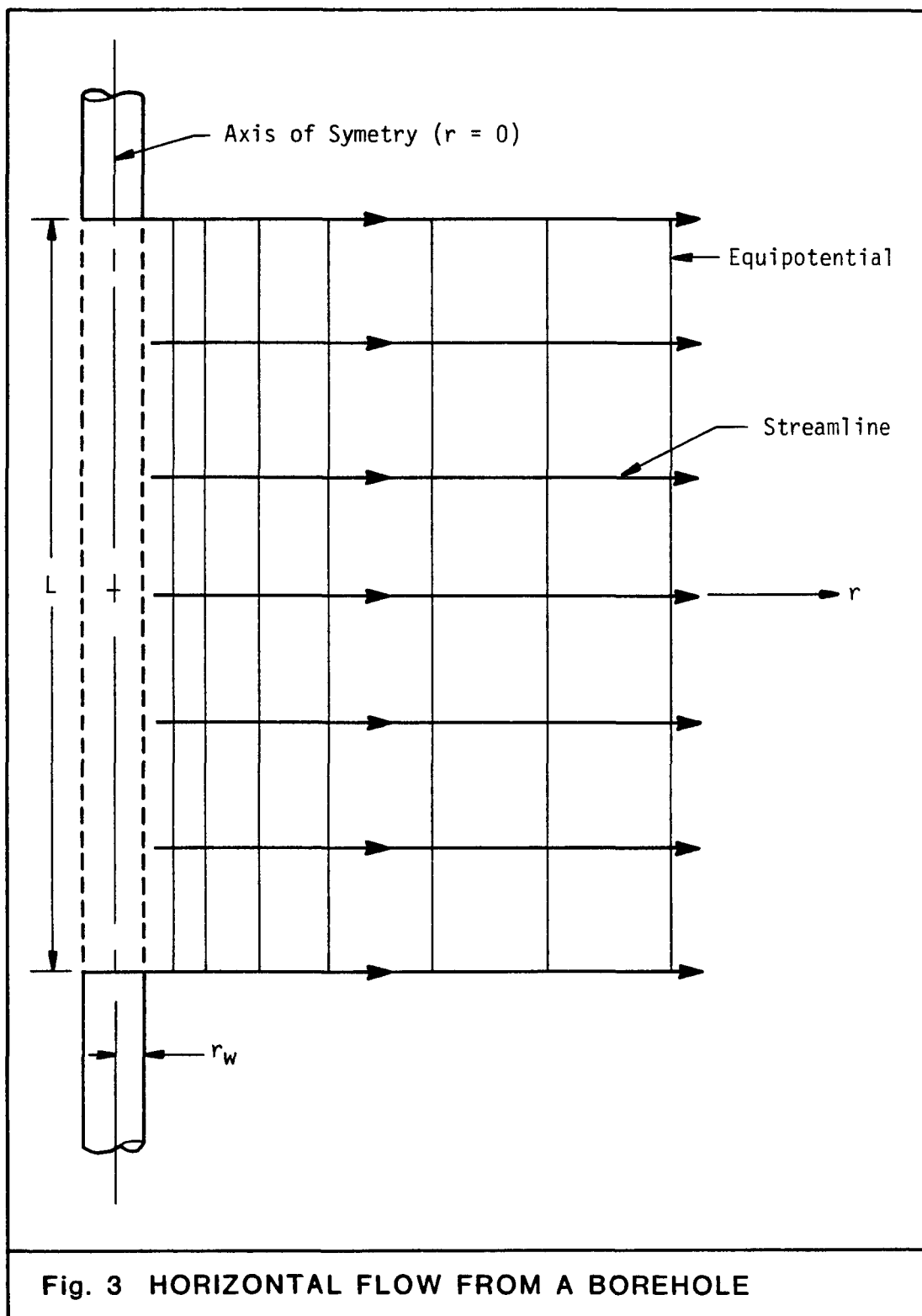
$$\delta(r_w, t) = \delta_0 \quad (2-20)$$

The problem defined by equations (2-17) through (2-20) was originally solved by Smith (1937) for the analogous heat flow problem and was adapted to hydrological units by Jacob and Lohman (1952). The problem was also solved independently by Van Everdingen and Hurst (1949).

Borehole flow rate is determined by applying Darcy's law at the borehole radius,

$$Q(t) = -2\pi K_r L r_w \frac{\partial \delta}{\partial r}(r_w, t) \quad (2-21)$$

The exact solution can be summarized as,



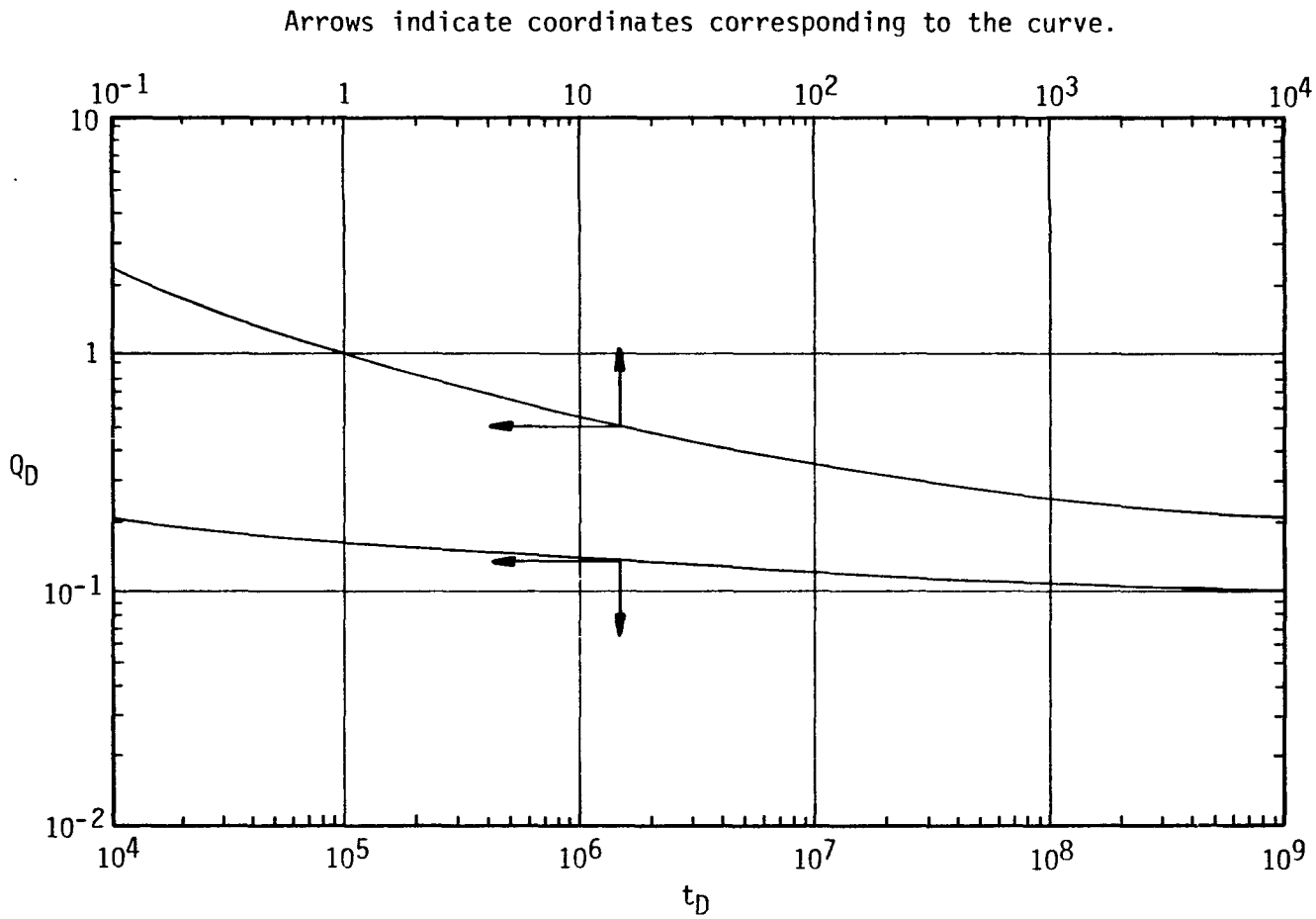
$$Q(t) = 2\pi K_r L \Delta_o Q_D(t_D) \quad (2-22)$$

where:

$$t_D = \frac{K_r t}{S_s r_w^2} \quad (2-23)$$

Q_D and t_D are parameters termed "dimensionless flow rate" and "dimensionless time," respectively. Their functional relationship is shown as a type curve in Figure 4.

Fig. 4 TYPE CURVE (Q_D vs. t_D) FOR STRICTLY HORIZONTAL FLOW



Note: Full size plot available in Lohman (1972)

CHAPTER 3

NUMERICAL ANALYSIS

A closed-form solution is not available for the mathematical problem defined by equations (2-11) through (2-16). Therefore, numerical solutions were obtained by modeling the flow region with the finite element program FLUMPS using a CYBER 175 computer. FLUMPS discretizes the space derivatives in the saturated flow equation (eq. 2-1) by a system of triangular elements based on the Galerkin method, and time derivatives are approximated with finite differences. The result is a system of simultaneous linear algebraic equations which are solved by either a point iterative or direct solution method. FLUMPS employs an adaptive explicit-implicit solution strategy so that nodes satisfying appropriate stability criteria are solved explicitly, leading to a considerable saving in computer time.

The size of a time step (Δt) is controlled automatically by various parameters including SIVARY, which is the maximum desired change in head during a time step. At every interior node, the change in head during the two previous time steps is used to estimate the projected change in head during the next time step for a given Δt . The actual size of the time step is then chosen so that, anywhere in the mesh, the predicted change in head is close to SIVARY but does not exceed two times SIVARY. When the time step is completed, the program calculates the changes in head which actually occurred, and if the

above limit is exceeded, the time step is repeated using a smaller Δt . As an additional check, the program calculates the global mass balance of the system during each time step. If the mass balance error exceeds a certain percent, the time step is repeated with a smaller Δt (Neuman and Narasimhan, 1977).

The printed output of FLUMPS provides information on the net flow rate into the exclusive subdomain of each node during a time step as well as flow rate across the boundaries of the flow region. Such information can be used to calculate the total flow rate across a given boundary during a time step. For more detailed information regarding the theoretical development and practical use of FLUMPS, the reader is referred to Neuman and Narasimhan (1977), Fogg (1979), Stephens (1979), and Neuman et al. (1982).

Input parameters were chosen to simulate conditions that might be encountered in the field. Isotropic hydraulic conductivity (K) and specific storage (S_s) were arbitrarily chosen as 10^{-4} cms^{-1} and 10^{-6} cm^{-1} , respectively. The borehole radius (r_w) was set equal to 5 cm and the prescribed hydraulic buildup (s_0) to 10 m.

It was assumed that the piezometer flow rate would be related to three dimensionless variables:

$$Q_D = \frac{Q}{2\pi K_r L s_0} \quad \text{dimensionless flow rate} \quad (3-1)$$

$$t_D = \frac{K_r t}{S_s R_w^2} = \frac{K_r t}{S_s r_w^2} \quad \text{dimensionless time} \quad (3-2)$$

$$\gamma = \frac{L}{2 R_w} = \frac{mL}{2 r_w} \quad (3-3)$$

The first two dimensionless variables are the same as those given by the Jacob-Lohman solution. The third dimensionless parameter (γ) is obtained from a steady-state analytical solution presented in Chapter 4. At various stages of the numerical simulation, parameters defining the dimensionless variables were altered to verify that Q_D was solely a function of t_D and γ . Thus, the following functional relationship was confirmed:

$$Q_D = f(t_D, \gamma) \quad (3-4)$$

3.1 Mesh Analysis

As a general rule, the accuracy of a numerical scheme increases as the finite element mesh is made finer. However, a finer mesh requires more elements and thus more computer time to simulate a given problem time. The practical application of the finite element method requires a compromise between desired accuracy and the efficient use of computer time. Mesh analysis is a procedure for selecting the coarsest mesh that produces a numerical solution of desired accuracy and computer efficiency. If the simulated problem has an exact analytical solution, the mesh is made successively finer until the numerical solution converges to the analytical solution. If an exact solution is not available, the mesh is made finer until the numerical solution ceases to change significantly, at which point an accurate solution is assumed.

Since the Galerkin method uses linear basis functions, a fine mesh was required near the borehole where large spatial changes in the

hydraulic gradient occur and a coarser mesh was acceptable far from the borehole where changes in the hydraulic gradient are small. The general approach was to design a relatively coarse "exterior mesh" which was not altered during the mesh analysis procedure. Between the open borehole face and the exterior mesh was an "interior mesh" which was made finer for each successive run. Since FLUMPS allows a completely arbitrary numbering system, the nodes and elements of the exterior mesh did not require renumbering as the interior mesh was altered. Elements of the mesh were composed of triangles and quadrilaterals. The program automatically divides each quadrilateral into two triangles by connecting two opposite corners with a line.

Interior meshes were designated A, B, or C depending on the dimensions of the square elements immediately adjacent to the borehole. An "A" mesh was the coarsest; its elements at the borehole were squares having the length r_w on each side. Meshes "B" and "C" were finer with element dimensions $r_w/2$ and $r_w/4$, respectively. All meshes were designed so that the size of the elements became gradually larger as distance from the open portion of the borehole increased.

In the discussion which follows, the (R, z) coordinate system is replaced by one based on the following parameters:

$$R_D = \frac{R}{R_w} \quad (3.1-1)$$

$$Z_D = \frac{z}{R_w} \quad (3.1-2)$$

where R_D and Z_D are dimensionless distances in the R and z directions, respectively.

3.2 Transient Horizontal Flow

To check the performance of FLUMPS and verify the basic modeling procedure, the first numerical simulation was for the case of transient horizontal flow in a homogeneous medium of infinite radial extent. This corresponds to a piezometer of infinite length ($\gamma = \infty$) or one which fully penetrates a horizontal stratum of constant thickness which is bounded above and below by impermeable boundaries. The exact analytical solution to this problem is given by the Jacob-Lohman solution previously discussed.

To completely define the problem in the flow region (R), all initial and boundary conditions must be specified (see Figure 5). Hydraulic buildup (s) is defined as the change in head from an initial steady-state condition. Therefore, any steady-state head distribution could be used as initial conditions for the numerical simulation. However, by letting,

$$h(R_D, Z_D, 0) = 0 \quad \text{in } R \quad (3.2-1)$$

the numerically determined head (h) became exactly equal to hydraulic buildup. Along Γ_1 , the open portion of the borehole, a constant hydraulic head (h_0) was prescribed,

$$h(1, Z_D, t) = h_0 \quad \text{on } \Gamma_1 \quad (3.2-2)$$

and on Γ_2 and Γ_3 , no-flow boundaries were specified,

$$\frac{\partial}{\partial Z_D} h(R_D, 8, t) = 0 \quad \text{on } \Gamma_2 \quad (3.2-3)$$

$$\frac{\partial}{\partial Z_D} h(R_D, 0, t) = 0 \quad \text{on } \Gamma_3 \quad (3.2-4)$$

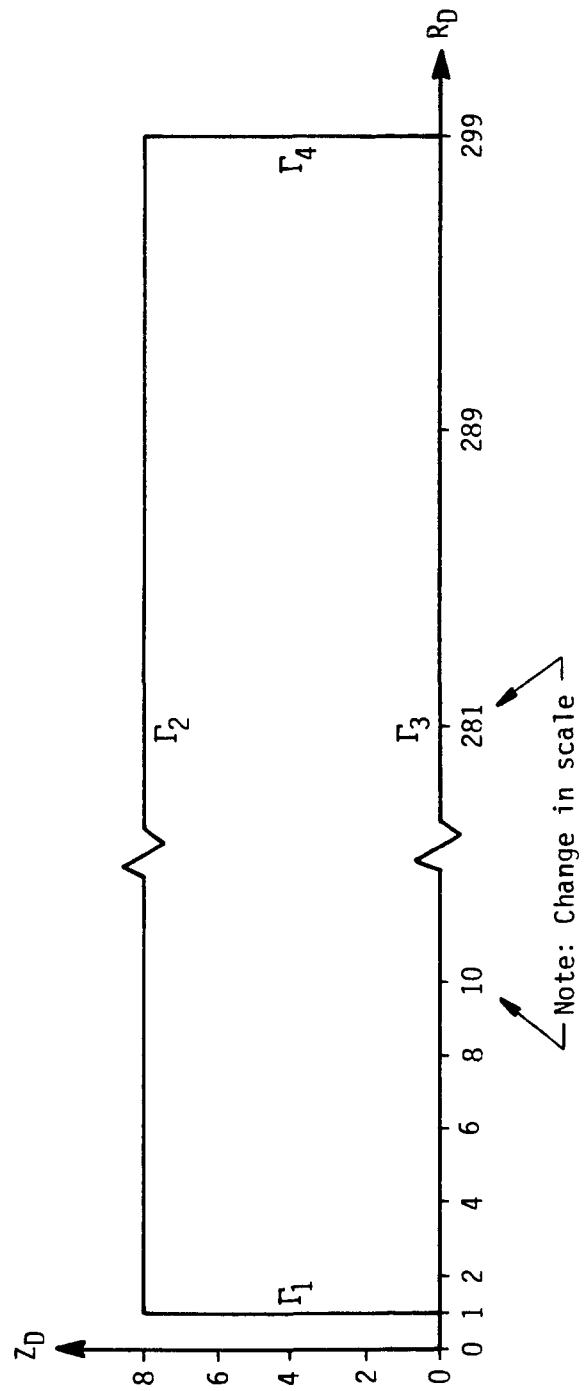


Fig. 5 BOUNDARY CONDITIONS FOR NUMERICAL SIMULATION OF STRICTLY HORIZONTAL FLOW

To approximate a medium of infinite radial extent, Γ_4 , was placed at a large radial distance, so that its presence had a negligible effect on the piezometer flow rate. Since negligible hydraulic buildup was expected at large radial distances throughout the simulation, this boundary was given a prescribed head of zero,

$$h(297, Z_D, t) = 0 \quad \text{on } \Gamma_4 \quad (3.2-5)$$

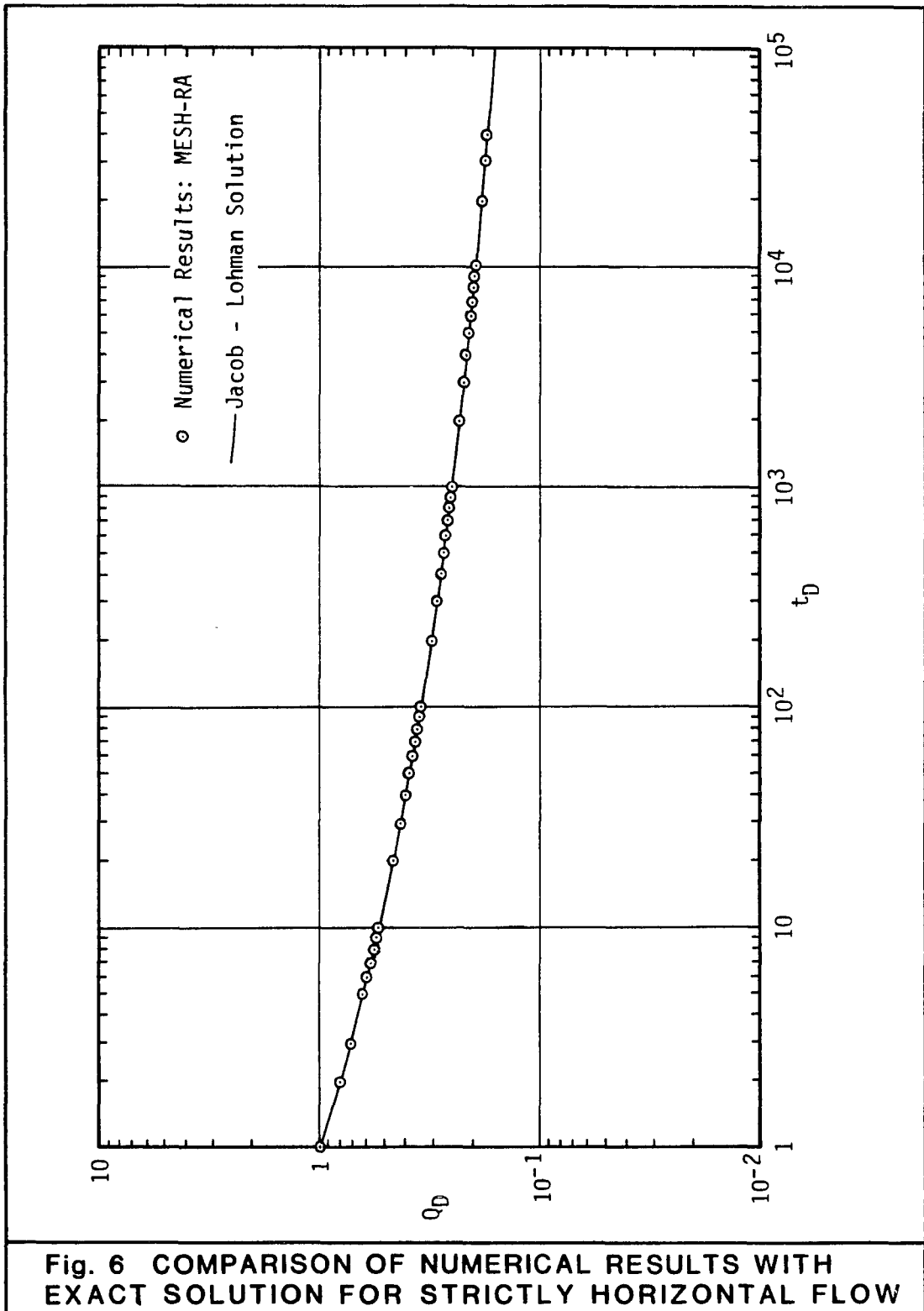
The external finite element mesh (MESH-R) and three internal meshes (A, B, and C) are shown in Plate 1. The composite meshes are designated MESH-RA, MESH-RB, AND MESH-RC (from coarser to finer).

Satisfactory results were obtained when SIVARY was set equal to 10.0 cm (one percent of the prescribed piezometer head). Computer printouts indicated almost identical Q_D - t_D values from each mesh for dimensionless time greater than one. As observed in Table 1, to simulate a total dimensionless time of 10^5 , MESH-RA required 11.6 seconds of computer time, compared to 14.4 seconds for MESH-RB and 22.5 seconds for MESH-RC. In all cases, the flux across boundary Γ_4 was negligible, indicating that an infinite medium had been adequately simulated. The numerical results of MESH-RA are compared to the Jacob-Lohman solution in Figure 6, where it is observed that the numerically derived values of Q_D and t_D are in excellent agreement with the exact analytical solution to the problem.

In this numerical simulation, FLUMPS proved to be an efficient program that was capable of accurate results for a problem of axially symmetric, saturated flow. It was further concluded that an "A" type mesh was sufficiently fine for the case of γ equal to infinity.

Table 1. Performance of FLUMPS in Simulating Strictly Horizontal Flow

	MESH-RA	MESH-RB	MESH-RC
Number of Elements	86	118	182
Number of Nodes	131	164	229
Total Dimensionless Time	10^5	10^5	10^5
Total Number of Time Steps	196	224	259
Total Computer Time (seconds)	11.6	14.4	22.5



3.3 Transient Nonhorizontal Flow

The next numerical simulation was for the case of transient nonhorizontal flow from a piezometer with the geometry $\gamma = 5$. Since an exact analytical solution is not available for this problem, the mesh analysis procedure was crucial for interpreting the accuracy of the numerical results.

The flow region and its associated boundaries are shown in Figure 7. Since the plane, $Z_D = 0$, is a plane of symmetry with respect to the flow field, only the region $Z_D > 0$ was considered in the numerical simulation. However, the flow rate calculated by the program was then one-half the actual piezometer flow rate. As in the previous case, the initial condition was,

$$h(R_D, Z_D, 0) = 0 \quad \text{in } R \quad (3.3-1)$$

Along Γ_1 (the open portion of the borehole) a constant piezometer head was prescribed,

$$h(1, Z_D, t) = h_0 \quad \text{on } \Gamma_1 \quad (3.3-2)$$

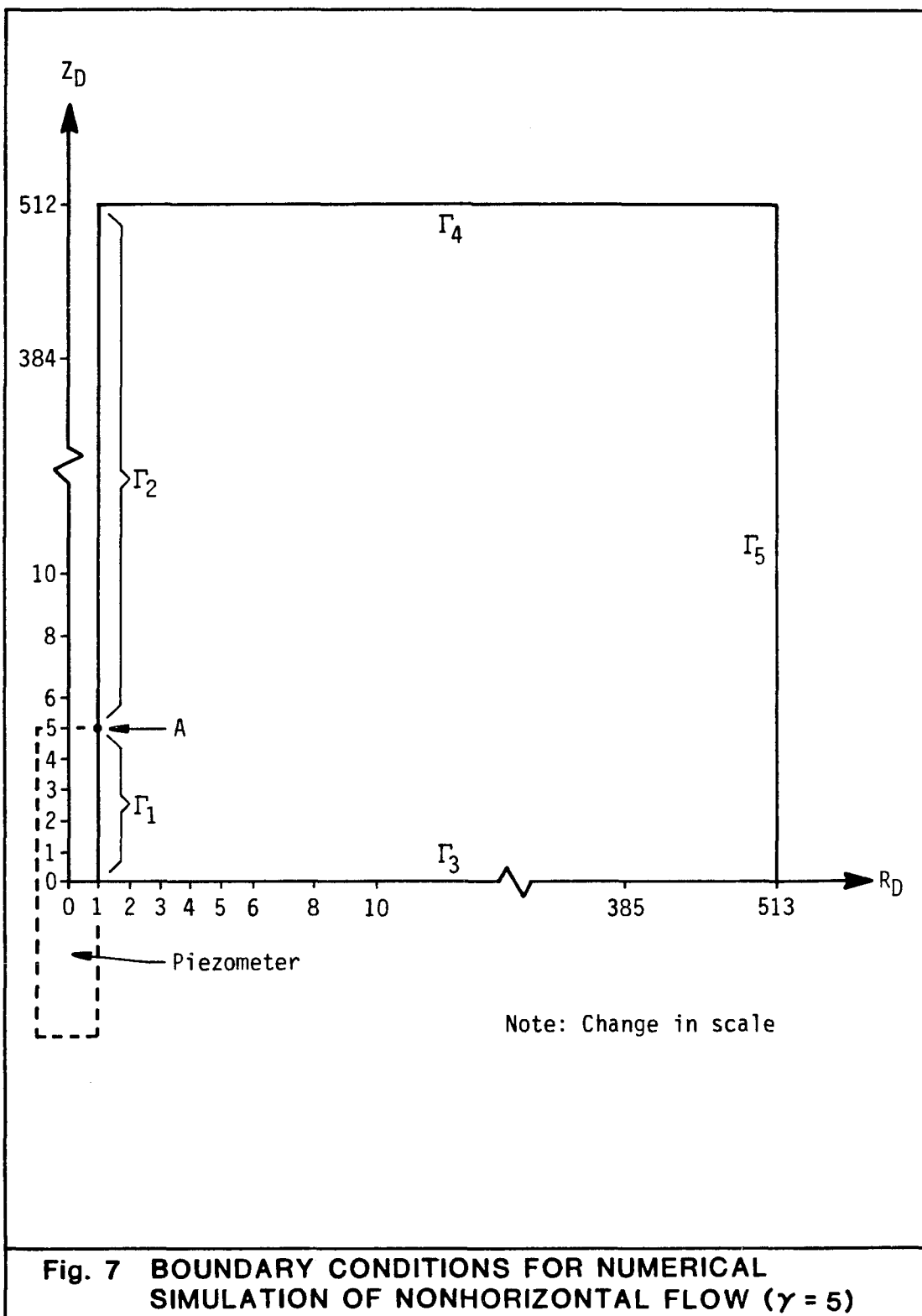
and Γ_2 was specified a no-flow boundary,

$$\frac{\partial}{\partial R_D} h(1, Z_D, t) = 0 \quad \text{on } \Gamma_2 \quad (3.3-3)$$

The flow direction would be parallel to the plane of symmetry represented by Γ_3 . Therefore, it was modeled as a no-flow boundary,

$$\frac{\partial}{\partial Z_D} h(R_D, 0, t) = 0 \quad \text{on } \Gamma_3 \quad (3.3-4)$$

Since the medium was assumed to have infinite thickness and radial extent, Γ_4 and Γ_5 were placed at large enough distances to have a negligible effect on the piezometer flow rate. Steady-state equations



for non-horizontal flow predict that when Z_D and R_D are greater than 500, the hydraulic buildup is less than five percent of the prescribed piezometer buildup. Steady-state conditions would exist at infinite time and therefore, for the case of transient flow, the formation buildup at this dimensionless distance would be less than the steady-state value. Therefore, the prescribed head boundaries, Γ_4 and Γ_5 were placed at $Z_D = 512$ and $R_D = 513$, respectively;

$$h(R_D, 512, t) = 0 \quad \text{on } \Gamma_4 \quad (3.3-5)$$

$$h(513, Z_D, t) = 0 \quad \text{on } \Gamma_5 \quad (3.3-6)$$

The exterior finite element mesh and three internal meshes are illustrated in Plate 2. The composite meshes are designated MESH-5A, MESH-5B, and MESH-5C (from coarser to finer).

Computer runs were made with each mesh and the results compared. Point "A" in Figure 7 represents a singularity point where the hydraulic gradient and flux rate both approach infinity. This is illustrated in Figure 2, where equipotentials are observed to "crowd together" near the end of the open borehole. The presence of the singularity point had a significant effect on the stability of the numerical scheme, causing the heads at nearby nodes to oscillate between time steps. Since FLUMPS used the change in head from preceding time steps to calculate the length of the next time step, the program tended to reduce Δt so that the amplitude of the oscillations would not exceed SIVARY. The numerical instability increased when the mesh was made finer in the vicinity of the singularity point, and as a result, there was a drastic increase in computer time for the finer meshes.

In Table 2, the performance of FLUMPS is compared for the three meshes. MESH-5A required 27.1 seconds of computer time and 269 time steps to simulate a dimensionless time of 4.0×10^4 . The runs for the two other meshes were aborted when 60 seconds of computer time had elapsed. At 60 seconds, MESH-5B simulated a dimensionless time of 3.3×10^3 in 350 time steps and MESH-5C simulated 1.7×10^2 in 1410 time steps. In both cases, FLUMPS controlled the amplitude of the oscillations by decreasing the time step, but this resulted in a great increase in computer time.

The numerical results of the three meshes are compared in Figure 8. The maximum variation in Q_D between the meshes is about 7% and the differences appear to decrease at larger times. The general trend was for the curve to shift downward slightly as the mesh was made finer. The discrepancies in the numerical results are not considered significant if one considers the uncertainties that would affect constant head tests performed in the field. It was therefore concluded that the "A" mesh was sufficiently fine to produce numerical results of desired accuracy for $\gamma = 5$. The numerical instability of the finer meshes made them impractical with regard to computer time. Since "A" meshes were acceptable for both $\gamma = 5$ and $\gamma = \infty$, it was further concluded that an "A" type mesh would be sufficiently fine for all piezometer geometries between those two values.

A general "A" mesh, containing 426 nodes and 417 triangular/quadrilateral elements, was designed to simulate borehole geometries with gamma values up to 50. Although the mesh was relatively efficient for the case of $\gamma = 50$, numerical instabilities became more

Table 2. Performance of FLUMPS in Simulating Nonhorizontal Flow
($\gamma = 5$)

	MESH-5A	MESH-5B	MESH-5C
Number of Elements	226	255	326
Number of Nodes	235	264	335
Total Dimensionless Time	4.0×10^4	3.3×10^3	1.7×10^2
Total Number of Time Steps	269	350	1410
Total Computer Time (seconds)	27.1	58.8	59.0

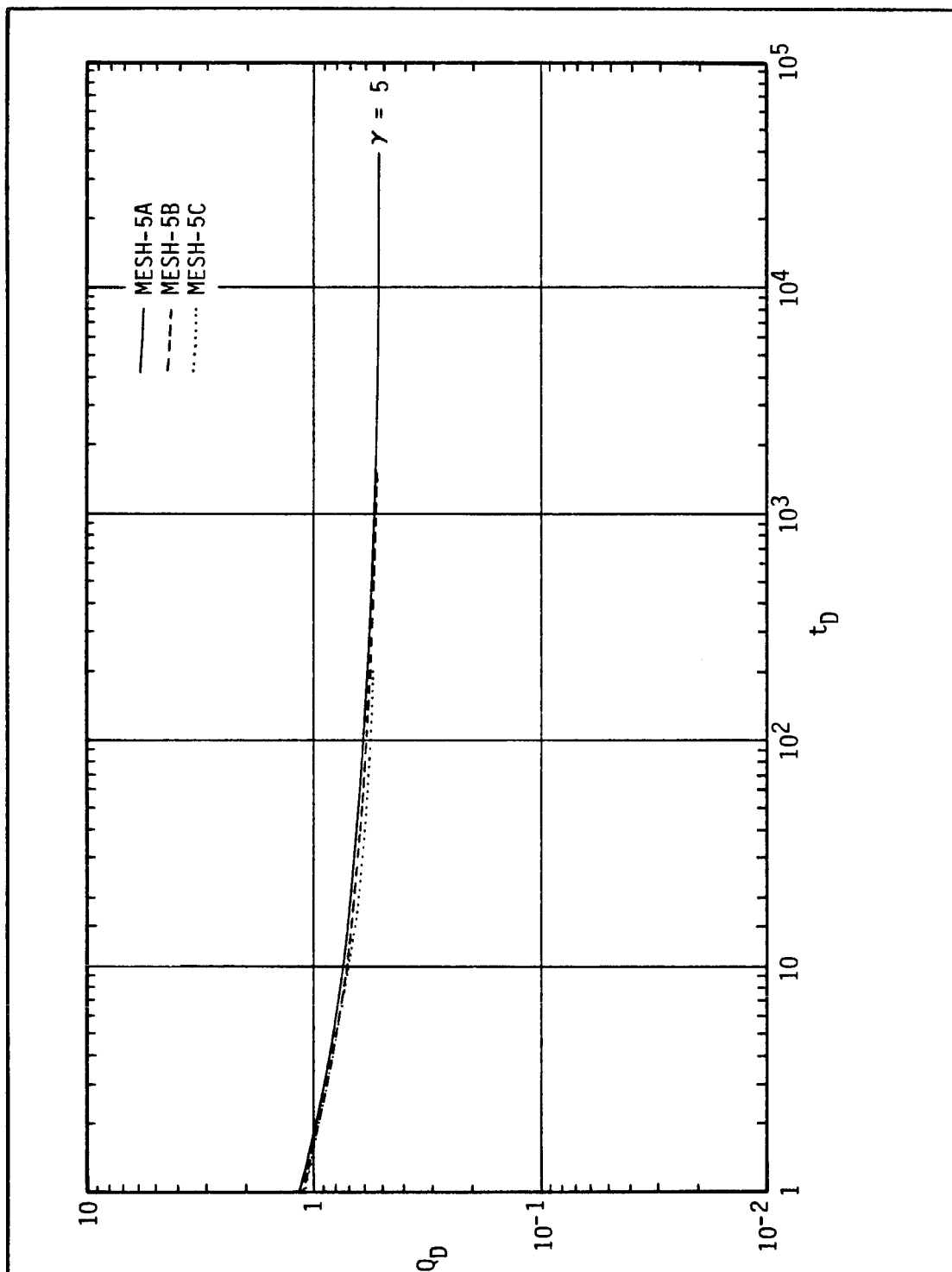


Fig. 8 COMPARISON OF NUMERICAL RESULTS FROM MESH-5A, MESH-5B, AND MESH-5C

significant as smaller gamma values were simulated, resulting in a drastic increase in computer time. Therefore, separate "A" meshes were designed for gamma values of 10 and 25. The numerical scheme continued to lose stability as gamma was reduced, but the corresponding numerical inefficiency was partially offset by a reduction in the number of nodes and elements (see Table 3). The numerical results are presented as a family of type curves in Figure 9, and a full-size plot is given in Plate 3.

3.4 Curve Matching Procedure for Determination of Hydraulic Conductivity

Jacob and Lohman (1952) describe a curve matching procedure for determining hydraulic conductivity from constant head tests performed in single, fully-penetrating boreholes ($\gamma = \infty$). The type curves in Figure 9 and Plate 3 can be used to extend their method for the more general case of a partially penetrating borehole in a medium of infinite thickness and radial extent. Field measurements of Q vs. t are graphed on logarithmic paper of the same scale as the type curves. While keeping the coordinate axes parallel, the field data is translated vertically and horizontally until a type curve is chosen which offers a "best fit." At any arbitrary match point, the values of Q'_D , t'_D , Q' , t' , and γ' are obtained. These match point values can be substituted into equations (3-1), (3-2), and (3-3) to calculate medium properties:

$$K_r = \frac{Q'}{2\pi L \Delta_0 Q'_D} \quad (3.4-1)$$

Table 3. Performance of FLUMPS for Each "A" Mesh

	MESH-5A	MESH-10A	MESH-25A	MESH-50A	MESH-RA
Number of Elements	226	254	352	499	86
Number of Nodes	235	236	361	508	131
Total Dimensionless Time	4.0×10^4	4.0×10^4	4.0×10^4	4.0×10^4	10^5
Total Number of Time Steps	269	263	297	297	196
Total Computer Time (seconds)	27.1	23.5	44.7	77.3	11.6

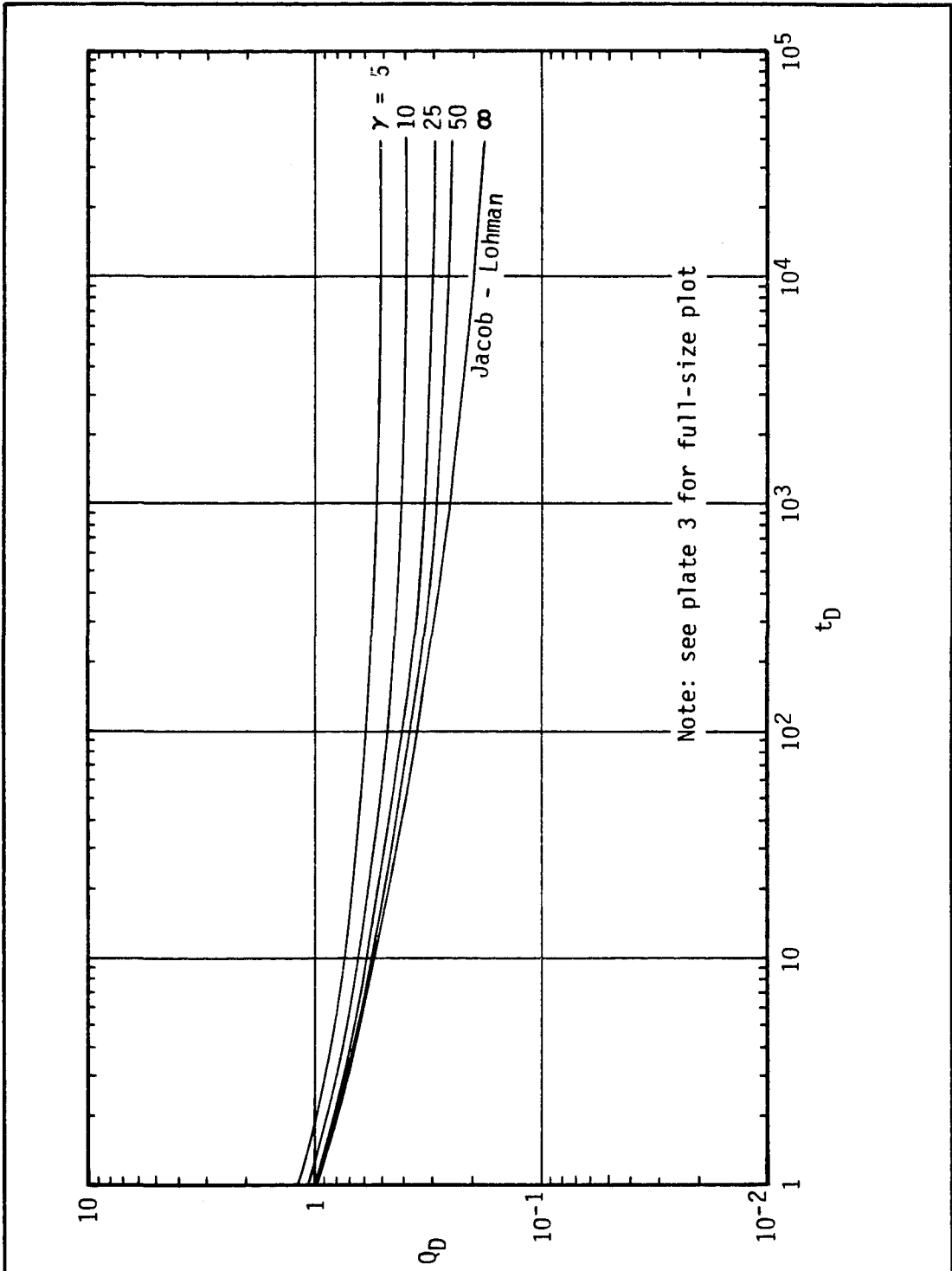


Fig. 9 TYPE CURVES (Q_D vs. t_D) FOR TRANSIENT NONHORIZONTAL FLOW

$$S_s = \frac{K_r t'}{r_w^2 t_D'} \quad (3.4-2)$$

$$m = \sqrt{\frac{K_r}{K_z}} = \frac{2 r_w \gamma'}{L} \quad (3.4-3)$$

Important limitations are inherent in the graphical procedure. Because the type curves have segments which are nearly flat, significant horizontal translation error can occur, which severely limits the reliability of calculated specific storage (eq. 3.4-2). In addition, the type curves have similar shapes for t_D' values of practical interest. It would therefore be very difficult to select one curve over another when an attempt is made to fit the field data. Selection of an improper curve would cause an error in the parameter m , and since K_z is proportional to the reciprocal of m^2 , a serious error in vertical hydraulic conductivity could result. It is therefore the author's opinion that a reliable determination of vertical hydraulic conductivity and specific storage cannot be made from constant head tests using a single borehole without observation piezometers.

The calculation of horizontal hydraulic conductivity requires the selection of a type curve, which ultimately depends on an assumed value of the parameter m . If the piezometer length is very large compared to its radius, the calculated value of K_r will not be sensitive to changes in m . For short piezometers, the selection of an improper value can lead to appreciable error in horizontal hydraulic conductivity. A hydrogeologic knowledge of the system may enable one to assign upper and lower bound values to m and in turn to the

calculated value of K_r . Such limits can be useful in many practical applications.

CHAPTER 4

STEADY-STATE ANALYSIS

At large values of dimensionless time, the type curves for smaller gamma values are nearly horizontal, indicating that the flow field near the piezometer is close to steady-state. Therefore, at large times a steady-state approximation should be sufficiently accurate for practical application. A steady-state approximation may not be valid for piezometers with large gamma values.

Hvorslev (1951) presented a series of equations to determine hydraulic conductivity from constant head tests in piezometers of various geometric shapes. For the piezometer or packer installations depicted in Figure 1, the most appropriate equation is as follows:

$$K_r = \frac{Q}{2\pi L \Delta s_0} \ln \left[\frac{mL}{2 r_w} + \sqrt{1 + \left(\frac{mL}{2 r_w}\right)^2} \right] \quad (4-1)$$

Hvorslev states the following assumptions:

1. uniform permeability
2. infinite soil depth
3. no disturbance, segregation, swelling or consolidation of soil
4. no air or gas in soil, well point, or pipe
5. negligible hydraulic losses in pipes, well point, or filter.

He further states that the approximation is based on replacing the cylindrical piezometer with an ellipsoid. Hvorslev describes the logarithmic term in (4.1) as the "shape factor" for that piezometer but does not present a derivation of this term.

Cornwell (in Zanger, 1953) derives an equation for steady-state flow from a borehole which leads to the Hvorslev equation. It is presented here with some modifications. Consider a continuous point source of strength b , under steady-state conditions, in an equivalent isotropic medium of infinite horizontal and vertical extent. The flow field is described by Darcy's law in spherical coordinates as,

$$b = - 4\pi K_r a^2 \frac{d\Delta}{da} \quad (4-2)$$

where a is spherical distance from the point. After integration, the boundary condition $\Delta(\infty) = 0$, is applied,

$$\Delta(a) = \frac{b}{4\pi K_r} \frac{1}{a} \quad (4-3)$$

For the transformed cylindrical coordinate system in Figure 10, the hydraulic buildup $\Delta(R,z)$ resulting from a point source at $(0,\xi)$ is determined by substituting,

$$a = \sqrt{R^2 + (z - \xi)^2} \quad (4-4)$$

$$\text{Then, } \Delta(R, z) = \frac{b}{4\pi K_r} \frac{1}{\sqrt{R^2 + (z - \xi)^2}} \quad (4-5)$$

Because Darcy's law is a linear differential equation with respect to s , the buildup resulting from two or more point sources is simply the sum of the buildups from each point source. Therefore, a piezometer of length L can be replaced with an equivalent line source of constant strength c per unit length as shown in Figure 10. In this case, the strength of an infinitesimal portion of the line source is equal to $c d\xi$. Then,

$$s(R, z) = \frac{c}{4\pi K_r} \int_{-\frac{L}{2}}^{\frac{L}{2}} \frac{d\xi}{\sqrt{R^2 + (z - \xi)^2}} \quad (4-6)$$

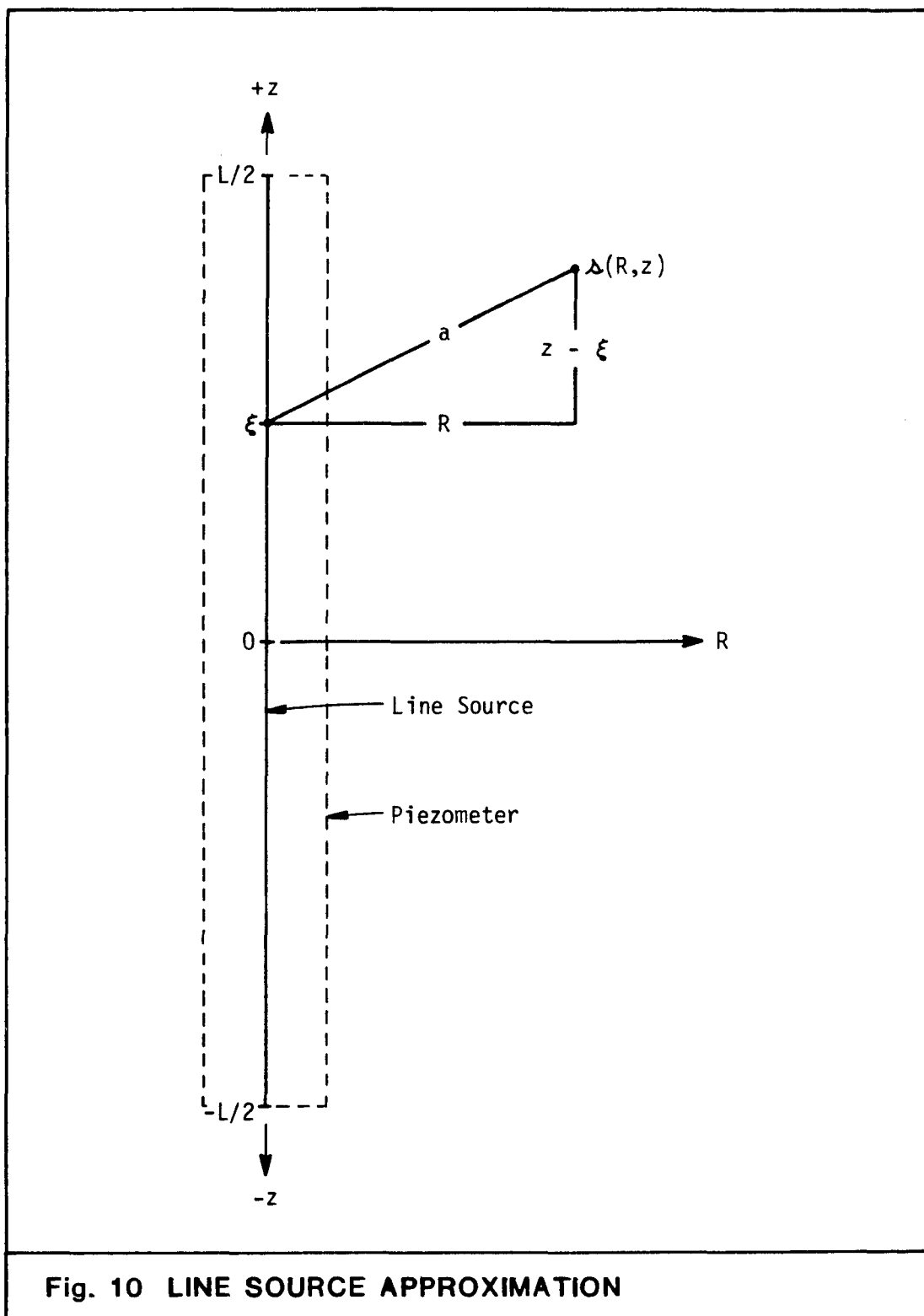
By letting $y = \xi - z$, the integral can be evaluated as follows:

$$\int_{-\frac{L}{2}}^{\frac{L}{2}} \frac{d\xi}{\sqrt{R^2 + (z - \xi)^2}} = \int_{-\frac{L}{2} - z}^{\frac{L}{2} - z} \frac{dy}{\sqrt{R^2 + y^2}} = \sinh^{-1} \left(\frac{y}{R} \right) \Bigg|_{-\frac{L}{2} - z}^{\frac{L}{2} - z} \quad (4-7)$$

Since c is a constant, the total flow rate is simply $Q = cL$. Making the appropriate substitutions and simplifying results in,

$$s(R, z) = \frac{Q}{4\pi K_r L} \left[\sinh^{-1} \left(\frac{\frac{L}{2} - z}{R} \right) + \sinh^{-1} \left(\frac{\frac{L}{2} + z}{R} \right) \right] \quad (4-8)$$

Equation (4-8) describes equipotential surfaces that have the shape of confocal prolate spheroids with foci at $(0, L/2)$ and $(0, -L/2)$. While this is a reasonable buildup distribution at some distance from the piezometer, it does not exactly describe the equipotential surface of the piezometer itself, which is a cylinder of length, L , radius r_w ,



and hydraulic buildup Δ_0 . To simulate this boundary condition, an ellipsoidal equipotential surface must be assigned the prescribed buildup in such a way that the flow rate is best approximated.

Approximation 1. Cornwell (and apparently Hvorslev) used the approximation $\Delta_0 = \Delta(R_w, 0)$ to simulate the actual boundary condition. In effect, the cylindrical piezometer is replaced with the prolate spheroid shown in Figure 11a. Substituting into (4-8) results in,

$$\Delta_0 = \frac{Q}{2\pi K_r L} \sinh^{-1} \left(\frac{L}{2R_w} \right) \quad (4-9)$$

The archyberbolic sine function has the following identity,

$$\sinh^{-1} (y) = \ln (y + \sqrt{1 + y^2}) \quad (4-10)$$

making this final substitution, where $y = L/2R_w = mL/2r_w$ and solving for K_r results in the Hvorslev equation,

$$K_r = \frac{Q}{2\pi L \Delta_0} \ln \left[\frac{mL}{2r_w} + \sqrt{1 + \left(\frac{mL}{2r_w}\right)^2} \right] \quad (4-1)$$

Approximation 2. If $\Delta_0 = \Delta(R_w, L/2)$, the piezometer is replaced by the prolate spheroid shown in fig. 11b. Then

$$\Delta_0 = \frac{Q}{4\pi K_r L} \left[\sinh^{-1} (0) + \sinh^{-1} \left(\frac{L}{R_w} \right) \right] \quad (4-11)$$

Simplifying and solving for K_r results in,

$$K_r = \frac{Q}{2\pi L \Delta_0} \frac{1}{2} \ln \left[\frac{mL}{r_w} + \sqrt{1 + \left(\frac{mL}{r_w}\right)^2} \right] \quad (4-12)$$

Approximation 3. The following approximation has been proposed by Neuman (personal communication),

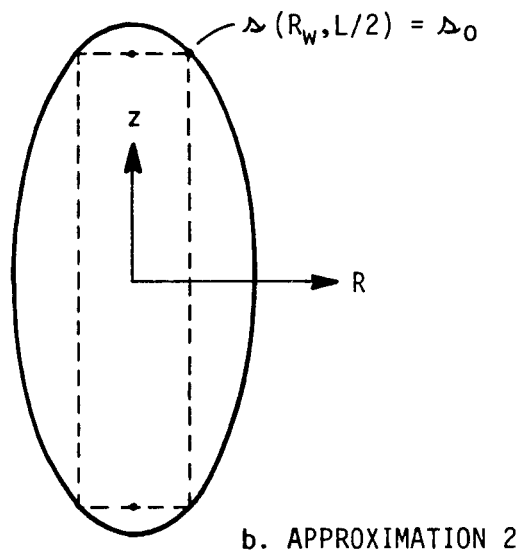
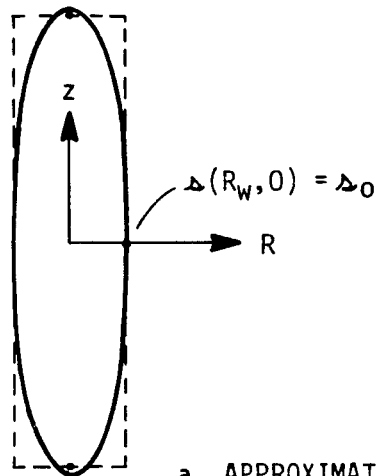


Fig. 11 CYLINDRICAL BOREHOLE APPROXIMATED WITH PROLATE SPHEROID

$$\Delta_0 = \frac{1}{L} \int_{-\frac{L}{2}}^{\frac{L}{2}} \Delta(R_w, z) dz \quad (4-13)$$

In this case, an averaged value of $\Delta(r_w, z)$ along the borehole face is assigned the prescribed buildup Δ_0 ,

$$\Delta_0 = \frac{Q}{4\pi K_r L^2} \left[\int_{-\frac{L}{2}}^{\frac{L}{2}} \sinh^{-1} \left(\frac{\frac{L}{2} - z}{R_w} \right) dz + \int_{-\frac{L}{2}}^{\frac{L}{2}} \sinh^{-1} \left(\frac{\frac{L}{2} + z}{R_w} \right) dz \right] \quad (4-14)$$

The definite integrals can be evaluated by noting that,

$$\int_a^b \sinh^{-1} \left(\frac{y}{R_w} \right) dy = \left[y \sinh^{-1} \left(\frac{y}{R_w} \right) - \sqrt{y^2 + R_w^2} \right]_a^b \quad (4-15)$$

In the first integral, $y = L/2 - z$ and in the second, $y = L/2 + z$.

Carrying out the interpretation gives,

$$\begin{aligned} \Delta_0 = \frac{Q}{4\pi K_r L^2} & \left[- \left(\frac{L}{2} - z \right) \sinh^{-1} \left(\frac{\frac{L}{2} - z}{R_w} \right) + \left(\frac{L}{2} + z \right) \sinh^{-1} \left(\frac{\frac{L}{2} + z}{R_w} \right) \right. \\ & \left. + \sqrt{\left(\frac{L}{2} - z \right)^2 + R_w^2} - \sqrt{\left(\frac{L}{2} + z \right)^2 + R_w^2} \right]_{-\frac{L}{2}}^{\frac{L}{2}} \quad (4-16) \end{aligned}$$

Simplifying and solving for K_r results in the final equation,

$$K_r = \frac{Q}{2\pi L \Delta_0} \left[\ln \left(\frac{mL}{r_w} + \sqrt{1 + \left(\frac{mL}{r_w} \right)^2} \right) - \sqrt{1 + \left(\frac{r_w}{mL} \right)^2} + \frac{r_w}{mL} \right] \quad (4-17)$$

The preceding analyses can be summarized by the following general equation,

$$K_r = \frac{Q}{2\pi L \Delta_0} C \quad (4-18)$$

where the shape factor (C) is a parameter that depends solely on the geometry of the cylindrical piezometer and the anisotropy of the medium. Since $\gamma = mL/2r_w$, the three approximations result in the following shape factors,

$$C_1 = \ln (\gamma + \sqrt{1 + \gamma^2}) \quad (4-19)$$

$$C_2 = \frac{1}{2} \ln (2\gamma + \sqrt{1 + 4\gamma^2}) \quad (4-20)$$

$$C_3 = \ln (2\gamma + \sqrt{1 + 4\gamma^2}) - \sqrt{1 + \frac{1}{4\gamma^2}} + \frac{1}{2\gamma} \quad (4-21)$$

4.1 Comparison with Numerical Results

Since $C = 1/Q_D$ at steady-state, a fourth shape factor (C_N) can be approximated by using the numerical values of Q_D at the largest simulated time. Values of this numerically derived shape factor are compared with the analytical shape factors in Figure 12. The numerical results suggest an error in Hvorslev's shape factor of 14 to 19 percent for gamma values between 5 and 50 and an error of 6 to 7.5 percent in the shape factor derived from approximation 3. Since values of Q_D would be expected to decrease slightly at larger times, C_N may underestimate the true shape factor by a small amount. Therefore the stated errors can be considered maximums.

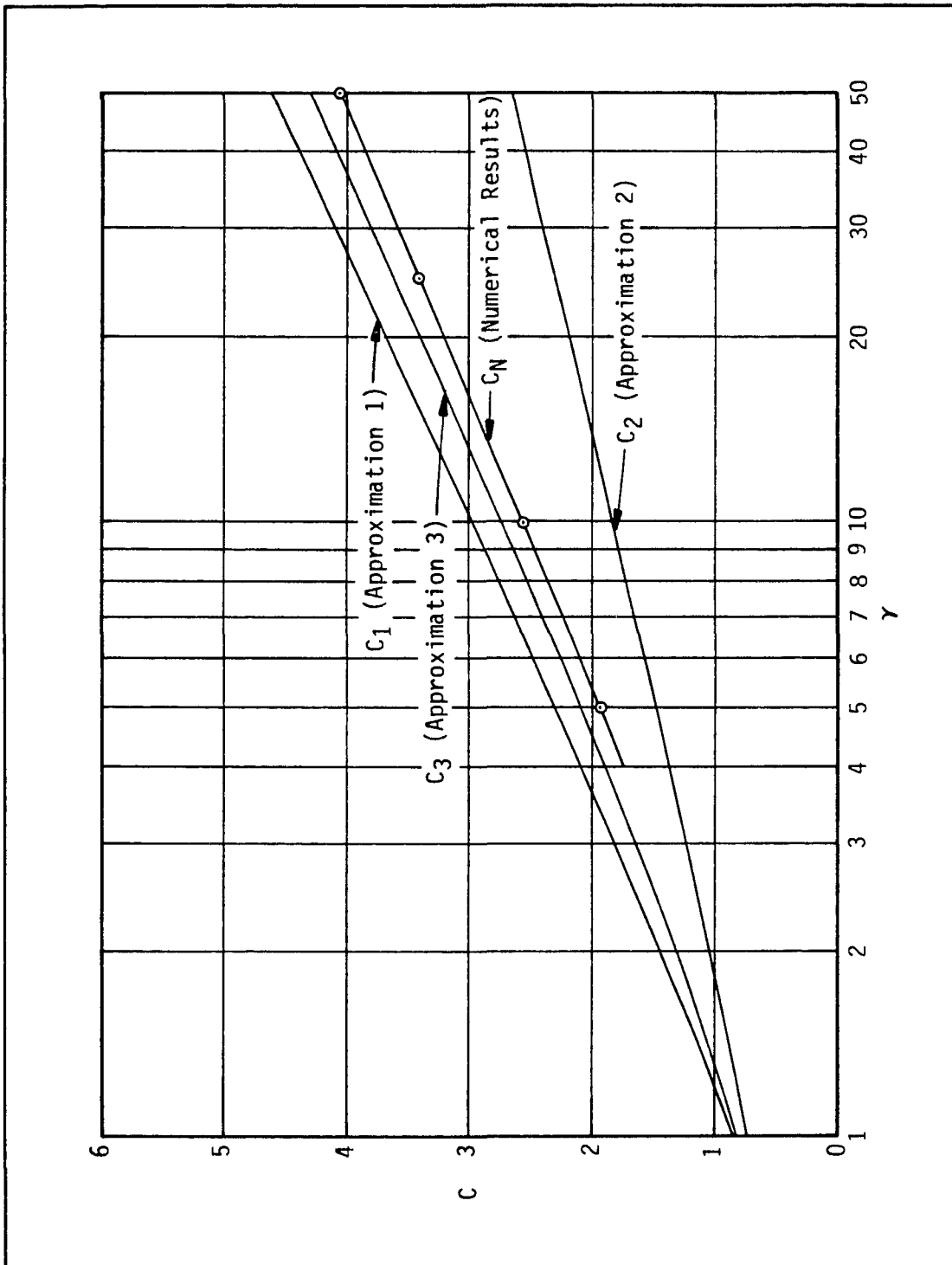


Fig. 12 COMPARISON OF NUMERICAL SHAPE FACTOR WITH ANALYTICAL APPROXIMATIONS

Values of the numerical shape factor plot as a straight line on semi-logarithmic paper and linear regression yields the following empirical relationship:

$$C_N \approx .923 \ln (\gamma) + .440 \quad (4.1-1)$$

where,

$$5 \leq \gamma \leq 50$$

Equation (4.1-1) is presented here as an improvement to the analytically derived shape factors.

As stated previously, the steady-state analytical approximations define equipotentials that have the shape of confocal prolate spheroids. A useful equation is obtained by dividing equation (4-8) by (4-18) and solving for the ratio (s/s_0) . In terms of dimensionless distances, the resulting equation is,

$$(s/s_0) = \frac{1}{2C} \left[\sinh^{-1} \left(\frac{\gamma + Z_D}{R_D} \right) + \sinh^{-1} \left(\frac{\gamma - Z_D}{R_D} \right) \right] \quad (4.1-2)$$

For approximation 3, the shape factor is given by equation (4-21). Figure 13 shows the distribution of hydraulic buildup given by (4.1-2) using shape factor C_3 for $\gamma = 10$. Figure 14 shows the buildup distribution given by the numerical results. The equipotentials for the two plots are quite different next to the borehole, but become more similar at increasing distances from the borehole. Although not shown, the equipotentials are almost identical for $(s/s_0) \leq 0.2$.

To evaluate the distribution of hydraulic flux along the borehole, the dimensionless flow rate contributed by a node at the borehole face is defined as,

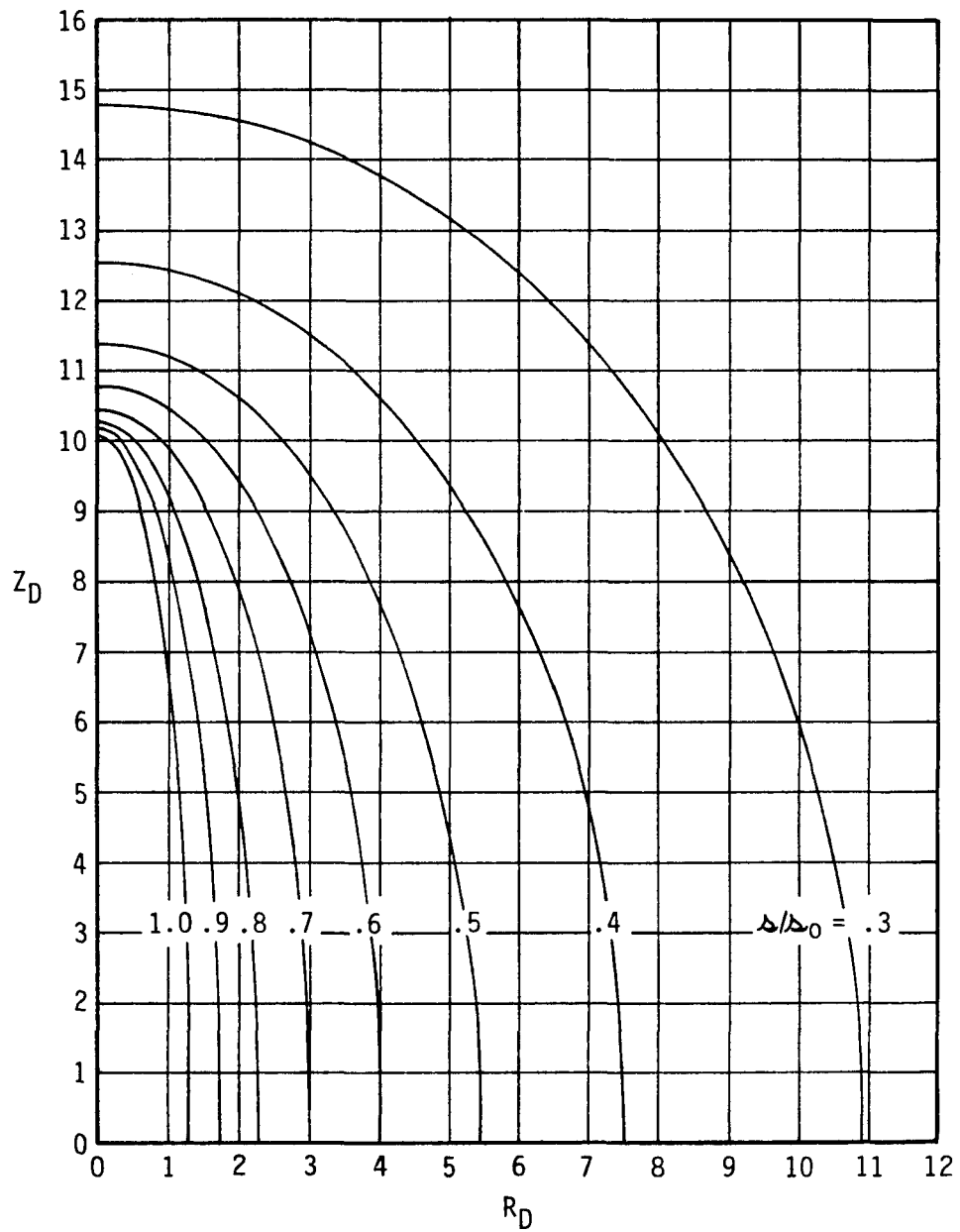


Fig. 13 STEADY-STATE HYDRAULIC BUILDUP DISTRIBUTION PREDICTED BY APPROXIMATION 3 ($\gamma = 10$)

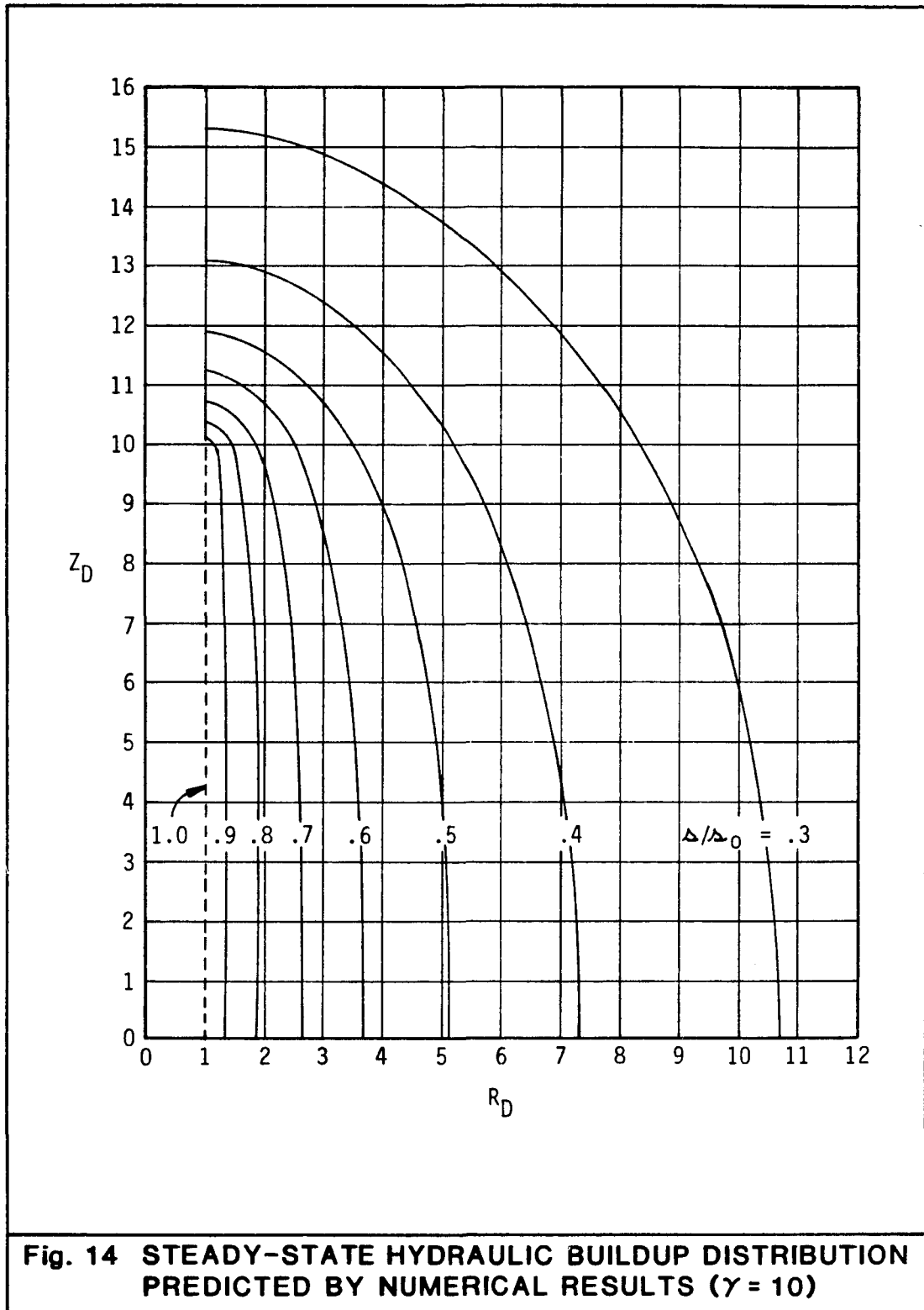


Fig. 14 STEADY-STATE HYDRAULIC BUILDUP DISTRIBUTION PREDICTED BY NUMERICAL RESULTS ($\gamma = 10$)

$$Q_{DN} = \frac{Q_N}{2\pi K_r \delta_0} \quad (4.1-3)$$

where Q_N is the volumetric flow rate per borehole length represented by the node. The sum of Q_{DN} , for all nodes defining the open portion of the borehole, is equal to Q_D . Figure 15 shows the distribution of flux along the borehole for various values of gamma based on the numerical results. At the singularity point, Q_{DN} assumes a large value, which is expected since the hydraulic gradient theoretically approaches infinity.

4.2 Multiple Rate Testing

When conducting permeability tests in a borehole, it is common practice to perform a series of tests at different prescribed heads. For steady-state conditions, equation (4-18) predicts a linear relationship between prescribed head (δ_0) and flow rate (Q), as shown in Figure 16a. In this case,

$$\delta_0 = \left(\frac{C}{2\pi K_r L} \right) Q = BQ \quad (4.2-1)$$

where B is the slope of the line. If field data plot as a straight line on a graph of δ_0 vs. Q, hydraulic conductivity can be calculated by solving B for K_r ,

$$K_r = \frac{C}{2\pi LB} \quad (4.2-2)$$

At higher flow rates, the graph is sometimes observed to deviate from a linear relationship, as shown in Figure 16b. This situation may result from nonlinear or turbulent flow inside the borehole

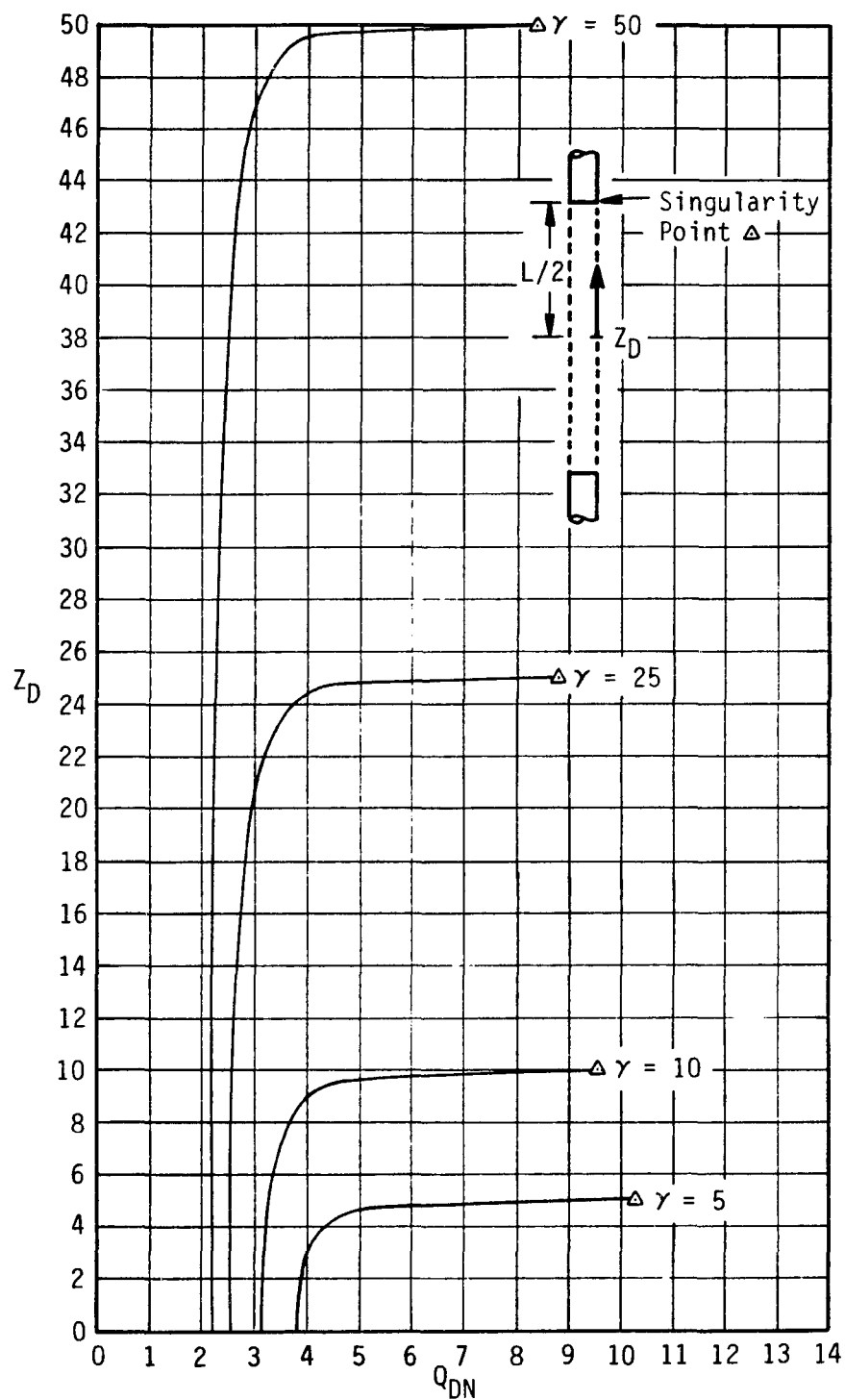
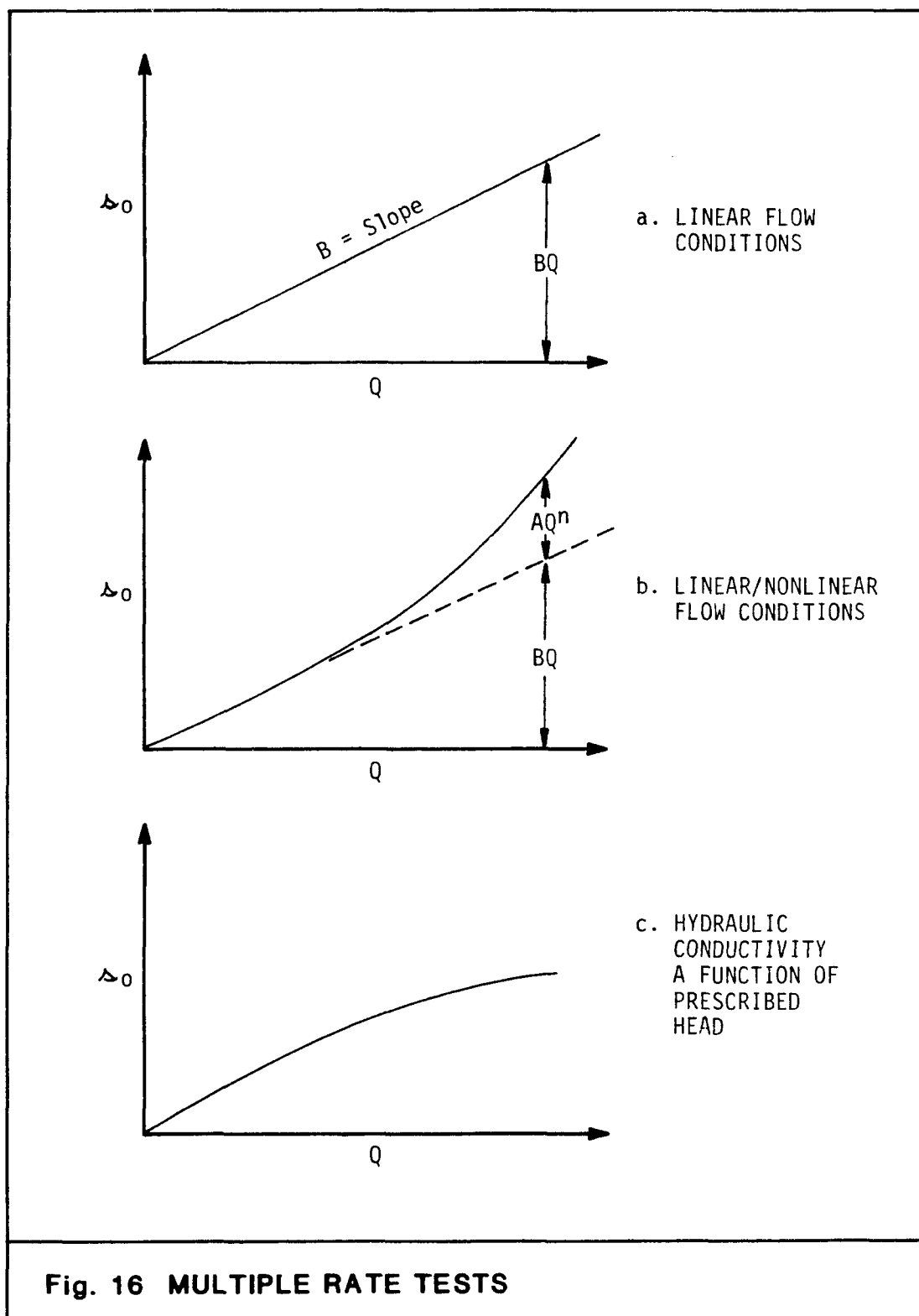


Fig. 15 DISTRIBUTION OF FLUX ALONG THE BOREHOLE



and/or within the medium near the borehole. Rorabaugh (1953) suggests the following equation for nonlinear flow conditions:

$$s_o = BQ + AQ^n \quad (4.2-3)$$

where A and n are empirical constants. The term BQ represents the hydraulic buildup resulting from linear flow and AQ^n is the additional buildup attributed to nonlinear flow. It is assumed that nonlinear flow is confined to a relatively narrow region adjacent to the borehole and that the remainder of the flow system is characterized by linear flow conditions (i.e., described by Darcy's law). Equation (4.2-3) can be rewritten as,

$$\log \left(\frac{s_o}{Q} - B \right) = (n-1) \log Q + \log A \quad (4.2-4)$$

which indicates that a plot of $\log (s_o/Q - B)$ vs. $\log Q$ should be a straight line, provided that the correct value of B is used.

Rorabaugh suggests the following procedure for calculating values of the unknown parameters:

1. Plots of $(s_o/Q - B)$ vs. Q are made on logarithmic paper for various values of B.
2. The value of B which yields a straight line is chosen and equation (4.2-2) is used to calculate K_r .
3. The slope of the line equals (n-1) and the intercept (at $Q=1$) is equal to A.

Values of n calculated by this method generally range from 2 to 3.

Figure 16c shows a graph for which hydraulic conductivity increases with prescribed head. This situation can occur in fractured

media where apertures increase as a result of higher pore pressure. The significance of turbulent flow cannot be interpreted from a response of this type.

4.3 Error Analysis

In a field situation, piezometer tests are subject to measurement errors. Borehole radius, or more specifically the "effective borehole radius" may be increased by drill bit wobble, caving of the borehole wall, and unintentional well development. It may be decreased by the infiltration of drilling fluids or development of a mudcake. Piezometer buildup may be overestimated due to head losses in the casing, well screen, or granular formation stabilizer, and flow rate is subject to error by the flow measuring device.

Consider a dependent variable Y which is a function of n independent random variables, each with a mean and a variance,

$$Y = g(X_1, X_2 \dots X_n) \quad (4.3-1)$$

If Y is expanded into a Taylor series, a first order approximation of its variance is given by,

$$\text{VAR} [Y] \approx \sum_{j=1}^n \left(\frac{\partial g}{\partial X_j} \right)^2 \text{VAR} [X_j] \quad (4.3-2)$$

where the derivatives are evaluated at the mean values of the independent variables (from Benjamin and Cornell, 1970, p. 184).

For steady-state conditions, the isotropic hydraulic conductivity is given by,

$$K = \frac{Q}{2\pi L \Delta_0} \left[.923 \ln\left(\frac{L}{2r_w}\right) + .440 \right] \quad (4.3-3)$$

If Q , δ_0 , and r_w are assumed to be independent random variables, the variance of K is approximated by,

$$\text{VAR} [K] \approx \left(\frac{1}{2\pi L \delta_0} \right)^2 \left[C_N^2 \text{VAR} [Q] + \left(\frac{Q C_N}{\delta_0} \right)^2 \text{VAR} [\delta_0] + .8519 \left(\frac{Q}{r_w} \right)^2 \text{VAR} [r_w] \right] \quad (4.3-4)$$

As an example, let the mean values of the variables be the parameter values used in the numerical simulation for $\gamma = 10$:

$$K = 10^{-4} \text{ cm s}^{-1}$$

$$\delta_0 = 1000 \text{ cm}$$

$$r_w = 5 \text{ cm}$$

$$L = 100 \text{ cm}$$

$$C_N = 2.56$$

and solving (4.3-3) for flow rate,

$$Q = 24.5 \text{ cm}^3 \text{ s}^{-1}$$

For this numerical example, assume the standard deviations of Q , δ_0 , and r_w are $1.5 \text{ cm}^3 \text{ s}^{-1}$, 20 cm , and 1 cm , respectively. The variances are,

$$\text{VAR} [Q] = (\text{SD}[Q])^2 = 2.25$$

$$\text{VAR} [\delta_0] = (\text{SD}[\delta_0])^2 = 400.$$

$$\text{VAR} [r_w] = (\text{SD}[r_w])^2 = 1.0$$

Substituting into (4.3-4),

$$\text{VAR} [K] \approx 9.33 \times 10^{-11}$$

and the standard deviation of K is,

$$\text{SD} [K] = \sqrt{\text{VAR}[K]} \approx 9.7 \times 10^{-6} \text{ cm s}^{-1}$$

which represents a random error in hydraulic conductivity of about 10%. In this example, the measurement errors in equation (4.3-3) would probably be unimportant compared to uncertainties in the physical model.

CHAPTER 5

CONCLUSIONS

A constant head test performed in a single, partially penetrating borehole is not considered an optimal method for determining hydraulic properties of a porous medium. Indeed the analytical and numerical solutions presented in this study point out significant limitations to the method. However, constant head tests can offer logistical advantages under certain field conditions, and thus the practicing hydrologist is commonly called on to analyze data of this type.

An exact analytical solution is given by Jacob and Lohman (1952) for the special case of transient horizontal flow from a fully penetrating borehole and Hvorslev (1951) presents a steady-state approximation for partially penetrating boreholes. Unfortunately, an exact analytical solution is not available for the general case of transient flow from partially penetrating boreholes. The purpose of this study has been to obtain a numerical solution for this more general case.

The following conclusions can be made, based on the numerical results:

- Reliable values of vertical hydraulic conductivity and specific storage cannot be determined from constant head

tests performed in single boreholes without observation piezometers.

- Calculated values of horizontal hydraulic conductivity have some degree of uncertainty because selection of a type curve (or shape factor) depends on an assumed value of the parameter m . This uncertainty can be reduced by constructing a piezometer with a large length-to-radius ratio.
- Approximately steady-state conditions are approached more rapidly in partially penetrating boreholes with small length-to-radius ratios. Following an initial transient period, a steady-state analysis is sufficiently accurate for practical application.
- Large amounts of time may be required for approximately steady-state conditions to exist in boreholes with large length-to-radius ratios. Fully penetrating boreholes never approach steady-state.
- A steady-state shape factor equation (derived from the numerical results) is presented as an improvement to that given by Hvorslev. However, Hvorslev's analytical shape factors differ from the numerical results by no more than 20 percent.
- In many field situations, the uncertainties resulting from measurement errors will probably be unimportant compared to uncertainties in the physical model.

Constant head pump tests are potentially useful from a logistical standpoint. However, the interpretation and analysis of test data requires a certain degree of caution.

APPENDIX

NOMENCLATURE

a = spherical distance (L)

A = empirical constant

b = strength of point source ($L^3 T^{-1}$)

B = slope of linear portion of (s_o vs. Q) graph (TL^{-2})

c = strength of line source per unit length ($L^2 T^{-1}$)

C = steady-state shape factor (dimensionless)

h = hydraulic head (L)

h_o = prescribed hydraulic head (L)

K = isotropic hydraulic conductivity (LT^{-1})

K_r = principal hydraulic conductivity in radial direction (LT^{-1})

K_z = principal hydraulic conductivity in vertical direction
(LT^{-1})

L = length of open portion of borehole (L)

$$m = \sqrt{\frac{K_r}{K_z}} \quad (\text{dimensionless})$$

n = empirical constant

Q = flow rate ($L^3 T^{-1}$)

Q' = flow rate at match point ($L^3 T^{-1}$)

$$Q_D = \frac{Q}{2\pi K_r L s_o} = \text{dimensionless flow rate (dimensionless)}$$

Q'_D = dimensionless flow rate at match point (dimensionless)

Q_N = flow rate per unit length contributed by node (L^2T^{-1})

Q_{DN} = dimensionless flow rate contributed by node (dimensionless)

r = radial distance (L)

r_w = radius of borehole (L)

$R = \frac{r}{m}$ = transformed radial distance for an equivalent isotropic medium (L)

$R_D = \frac{R}{R_w}$ = dimensionless radial distance for an equivalent isotropic medium (dimensionless)

R_w = transformed borehole radius for an equivalent isotropic medium (L)

δ = hydraulic buildup (L)

δ_0 = prescribed borehole hydraulic buildup (L)

S_s = specific storage (L^{-1})

$S_s^* = m^2 S_s$ = transformed specific storage for an equivalent isotropic medium (L^{-1})

$SD[Y]$ = standard deviation of the random variable Y

t = time (T)

t' = time at match point (T)

$t_D = \frac{K_r t}{S_s^* R_w^2} = \frac{K_r t}{S_s r_w^2}$ = dimensionless time (dimensionless)

t_D' = dimensionless time at match point (dimensionless)

$VAR [Y]$ = variance of the random variable Y

z = vertical coordinate (L)

$Z_D = \frac{z}{R_w}$ = dimensionless vertical distance (dimensionless)

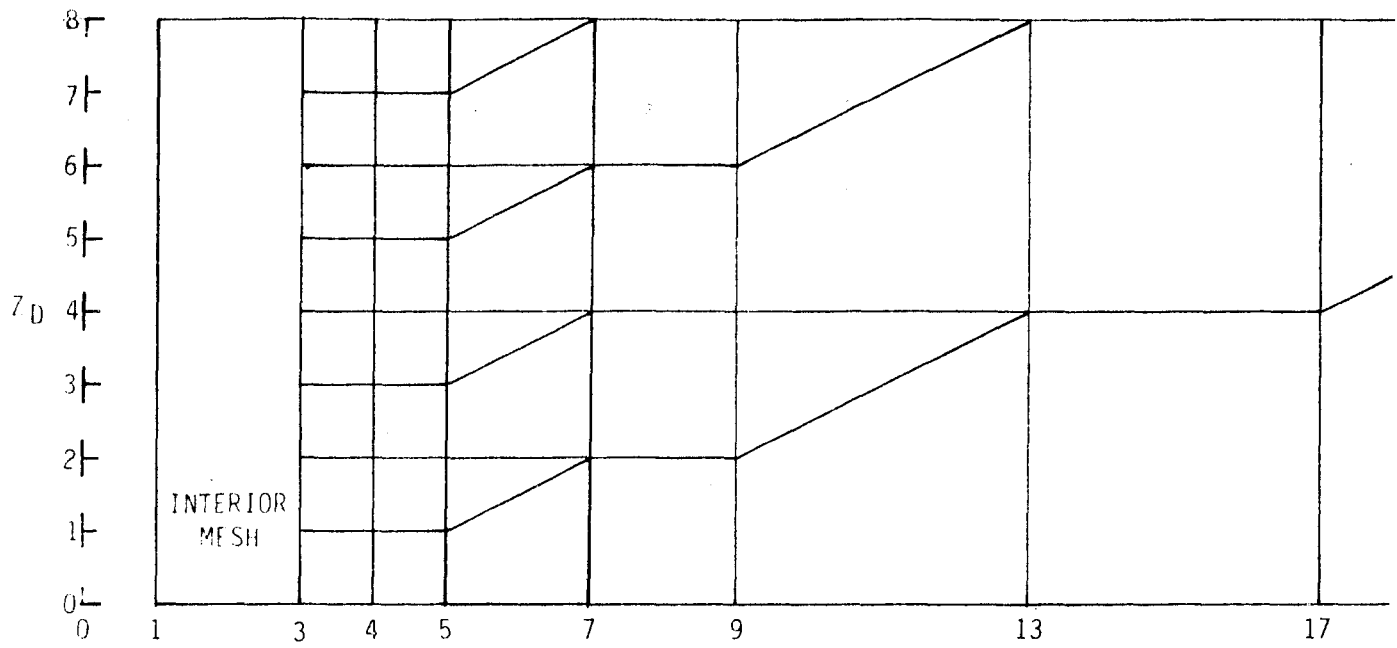
$$\gamma = \frac{L}{2R_w} = \frac{mL}{2r_w} \text{ (dimensionless)}$$

γ' = value of gamma for selected type curve (dimensionless)

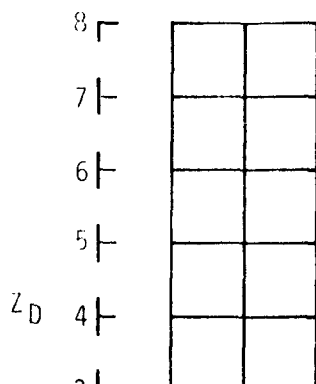
LIST OF REFERENCES

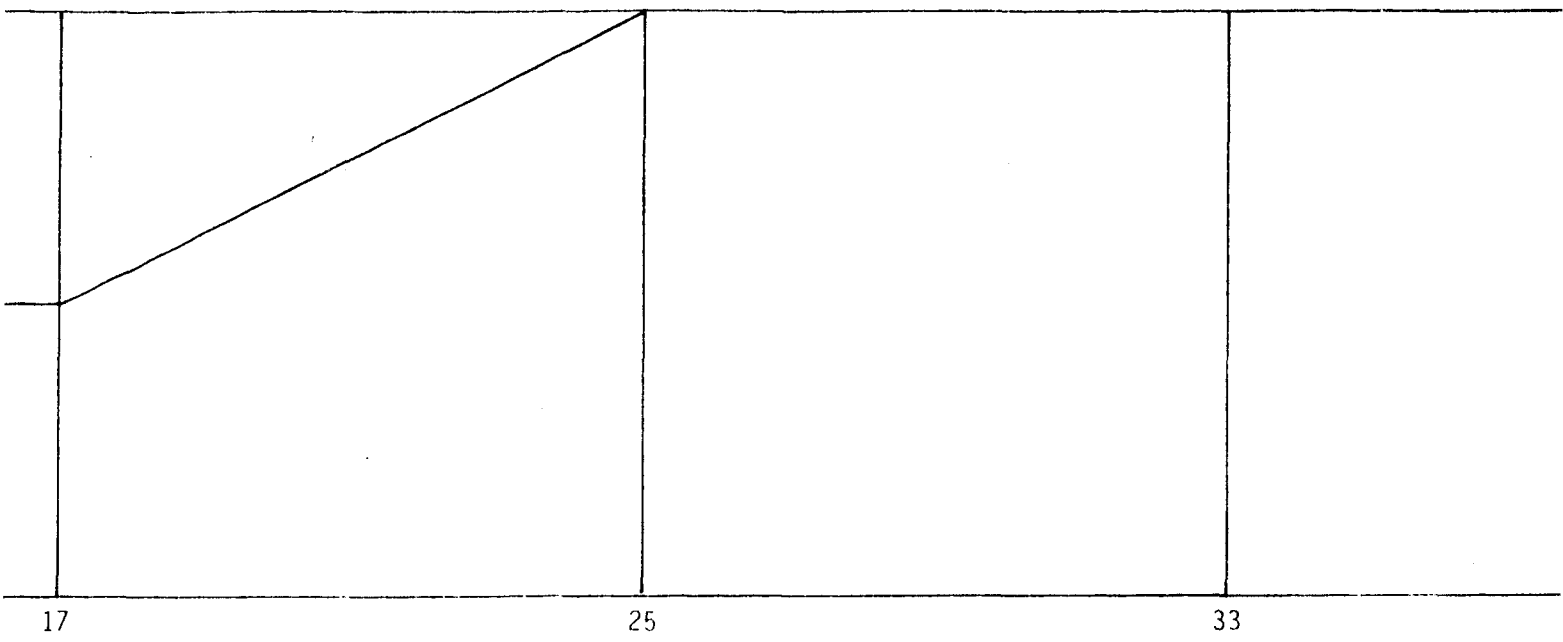
- Benjamin, J.R. and C.A. Cornell, 1970, Probability, Statistics, and Decision for Civil Engineers, McGraw-Hill Inc., New York, 684 p.
- Fogg, G.E., E.S. Simpson, and S.P. Neuman, 1979, Aquifer modeling by numerical methods applied to an Arizona groundwater basin, University of Arizona Technical Reports on Natural Resource Systems, Technical Report No. 32, 140 p.
- Hvorslev, M.J., 1951, Time lag and soil permeability in ground-water observations, U.S. Army Corps of Engineers, Waterways Experiment Station, Vicksburg, Mississippi, Bull. No. 36, 50 p.
- Jacob, C.E. and S.W. Lohman, 1952, Nonsteady flow to a well of constant drawdown in an extensive aquifer, Am. Geophys. Union Trans., vol. 33, pp. 559-569.
- Lohman, S.W., 1972, Ground-water hydraulics, U.S. Geol. Survey Prof. Paper 708, U.S. Government Printing Office, Washington D.C., 70 p.
- Neuman, S.P., Department of Hydrology and Water Resources, University of Arizona, Tucson, Arizona, 85721.
- Neuman, S.P. and T.N. Narasimhan, 1977, Mixed explicit-implicit iterative finite element scheme for diffusion-type problems, 1, theory, Int. J. Numer. Method. Eng., vol. 11, pp. 309-323.

- Neuman, S.P., C. Preller, and T.N. Narasimhan, 1982, Adaptive explicit-implicit quasi three dimensional finite element model of flow and subsidence in multiaquifer systems, *Water Resources Research*, vol. 18, no. 5, pp. 1551-1561.
- Rorabaugh, M.I., 1953, Graphical and theoretical analysis of step-drawdown test of artesian well, *Proc. Am. Soc. Civil Engineers*, vol. 79, separate no. 362, 23 p.
- Smith, L.P., 1937, Heat flow in an infinite solid bounded internally by a cylinder, *J. Appl. Phys.*, vol. 8, pp. 519, 524.
- Stephens, D.B., 1979, Analysis of constant head borehole infiltration tests in the vadose zone, University of Arizona Ph.D. thesis, 366 p.
- Van Everdingen, A.F. and W. Hurst, 1949, The application of the Laplace transformation to flow problems in reservoirs, *Trans., AIME*, vol. 186, pp. 305-324.
- Zanger, C.N., 1953, Theory and problems of water percolation, U.S. Bur. Rec. Engineering Monograph No. 8, 76 p.

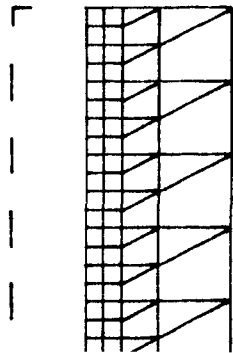
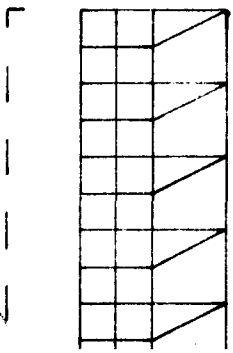


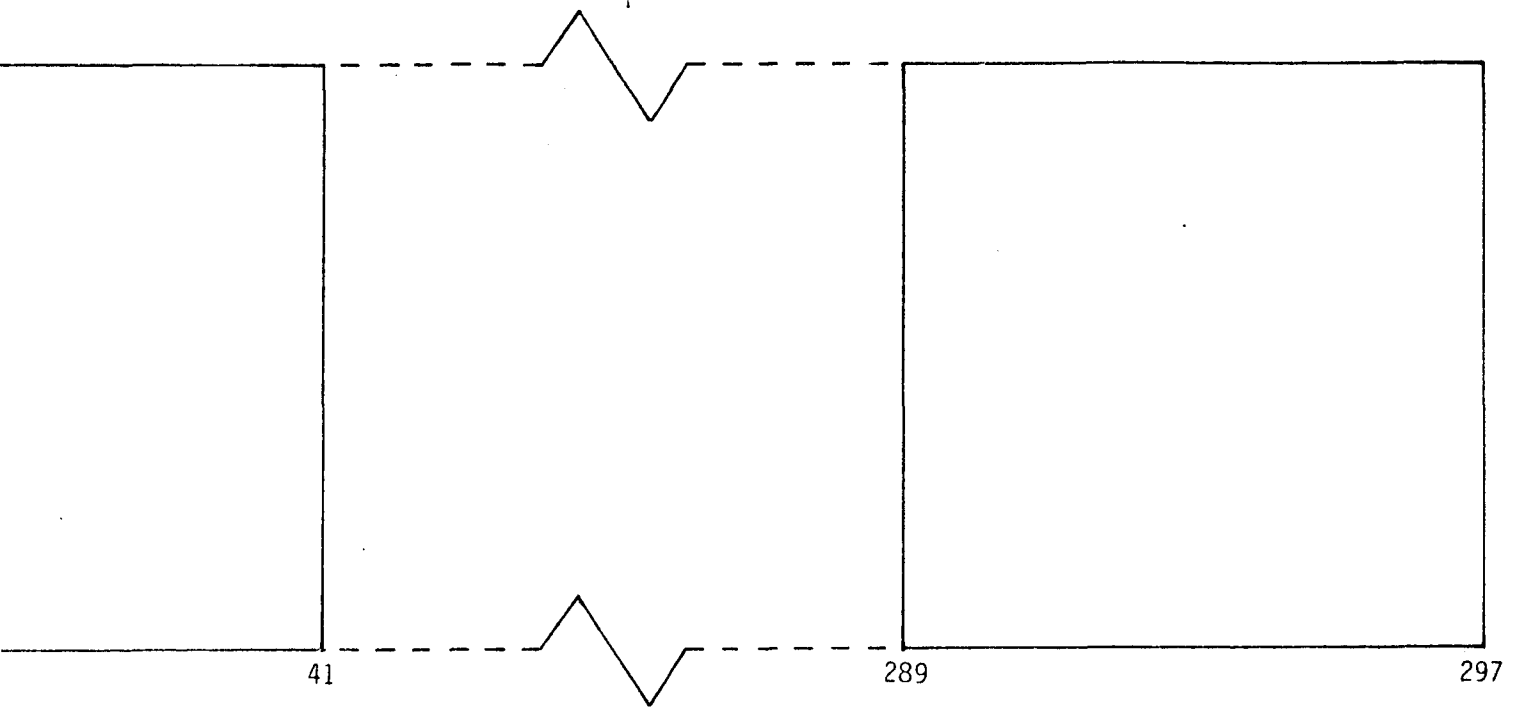
INTERIOR MESHES



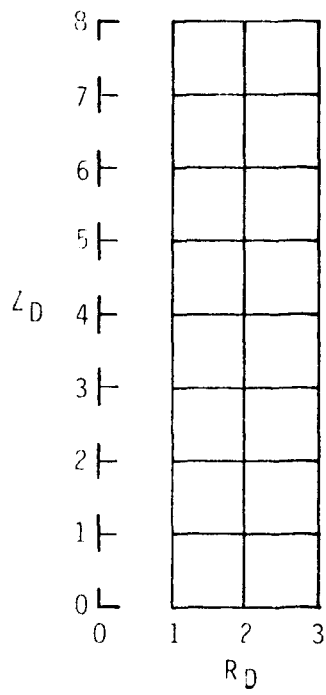


R_D

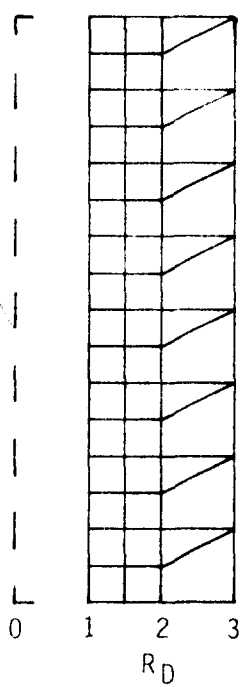




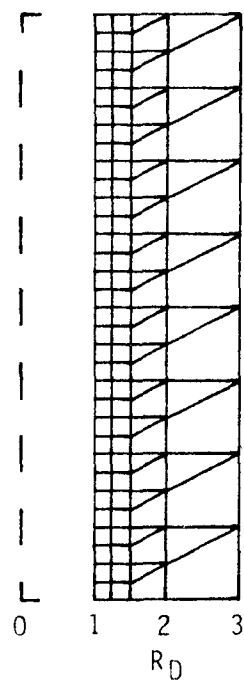
INTERIOR
MESHERS



MESH-RA



MESH-RB



MESH-RC

PLATE I. EXTERIOR MESH AND INTERIOR MESHES FOR STRICTLY HORIZONTAL

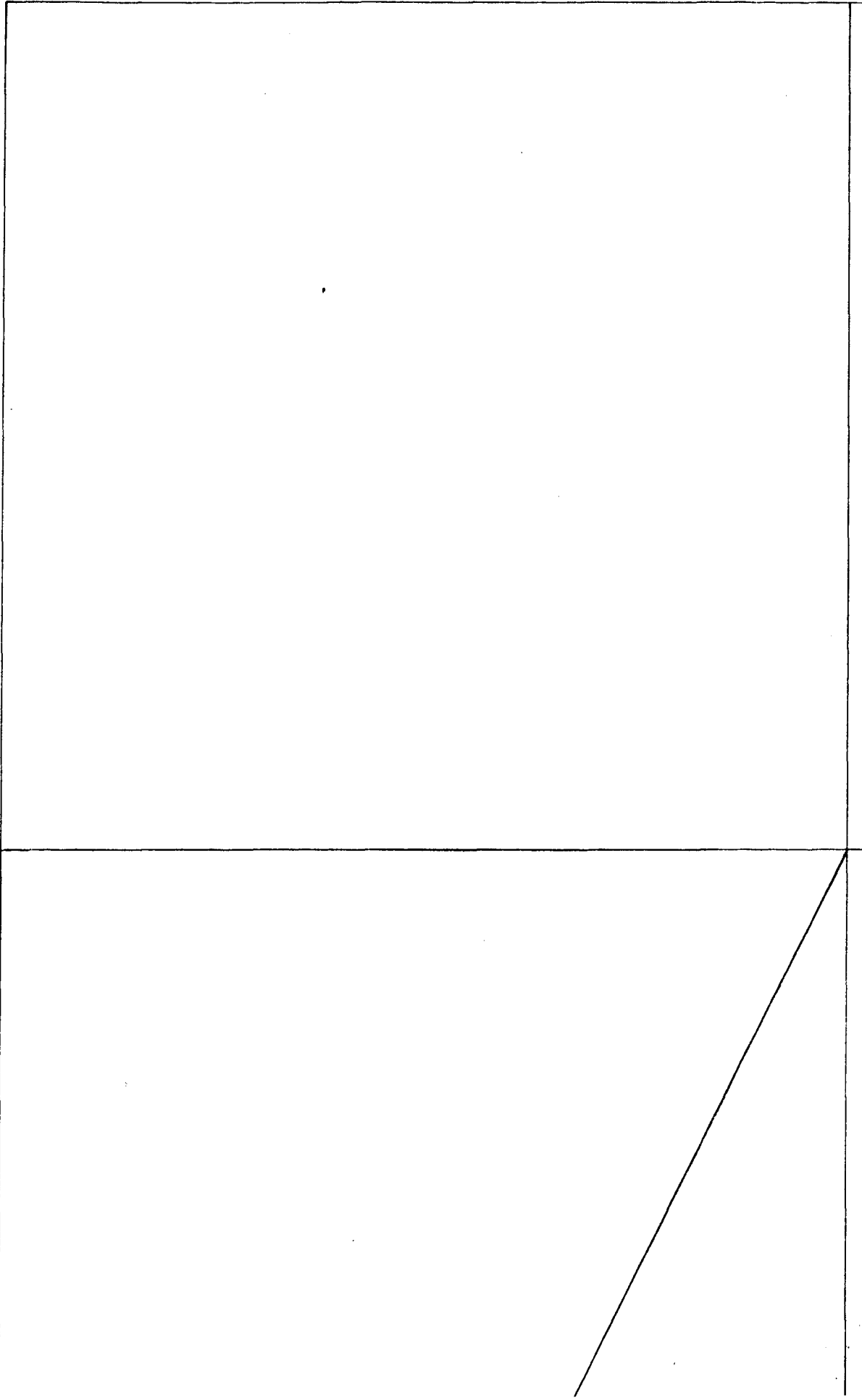
(F. Marinelli, M.S. Thesis, Department of Hydrology and Water Resources,

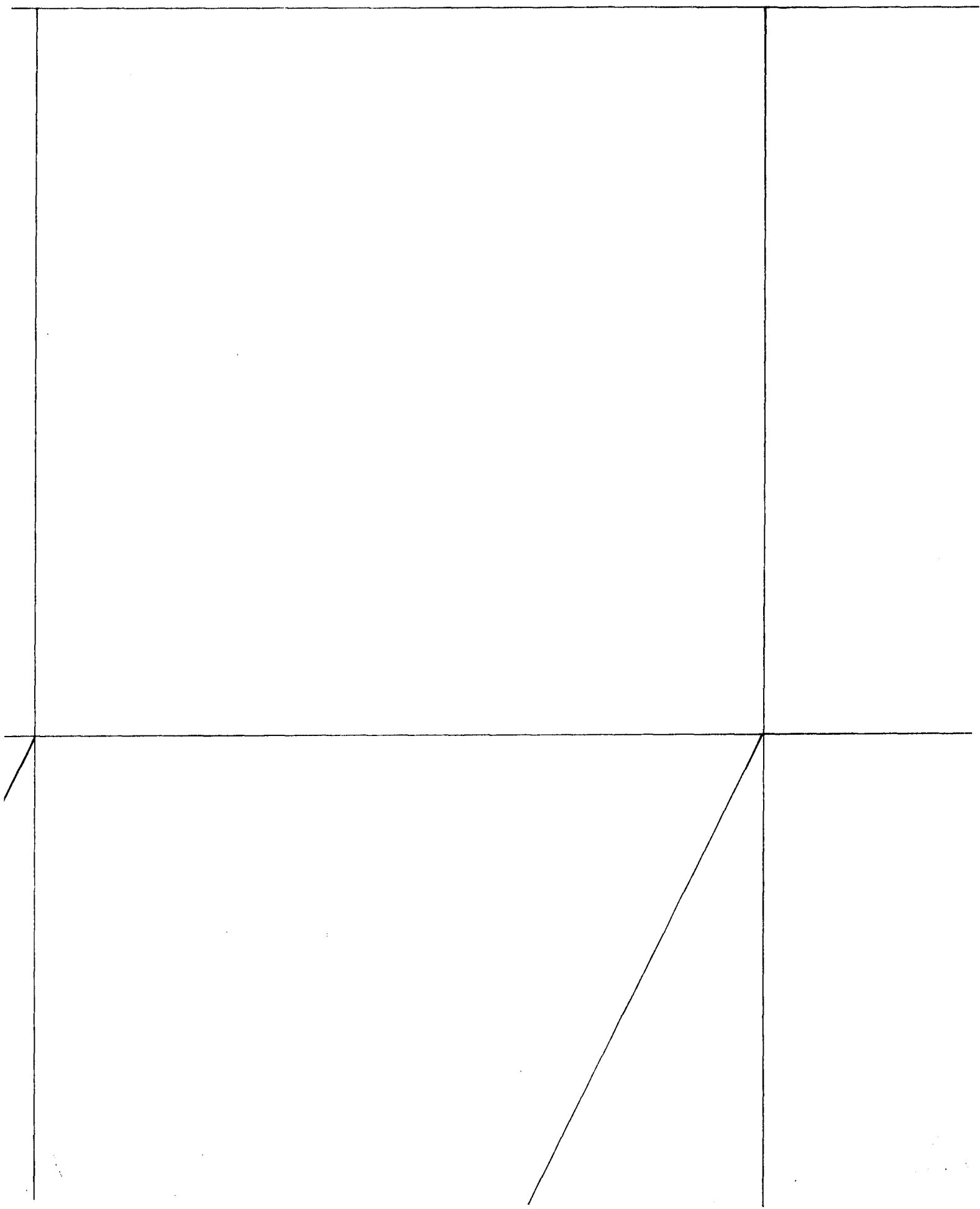
ZONTAL FLOW

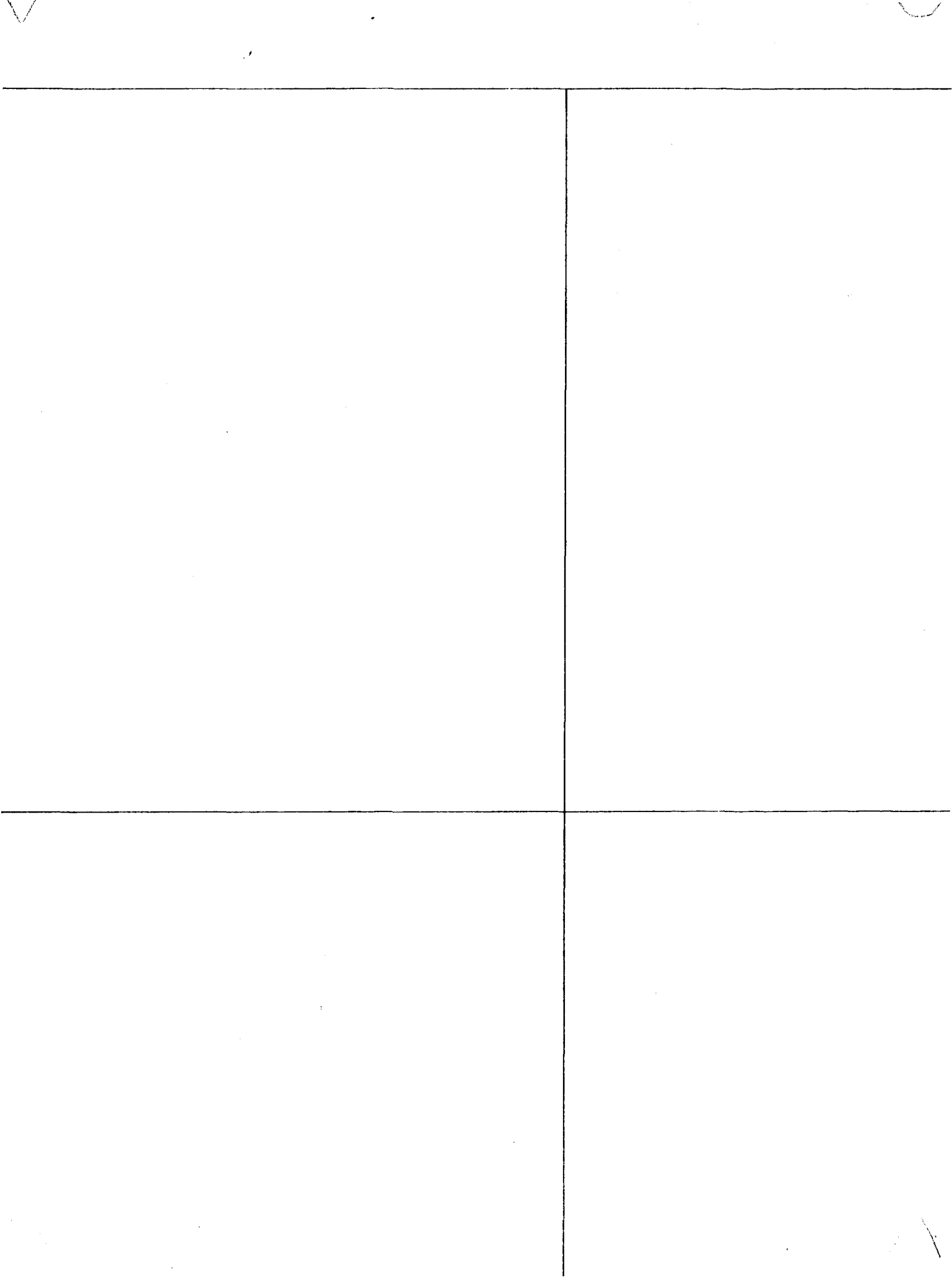
ces, University of Arizona, 1984)

512

384







z_D

256

192

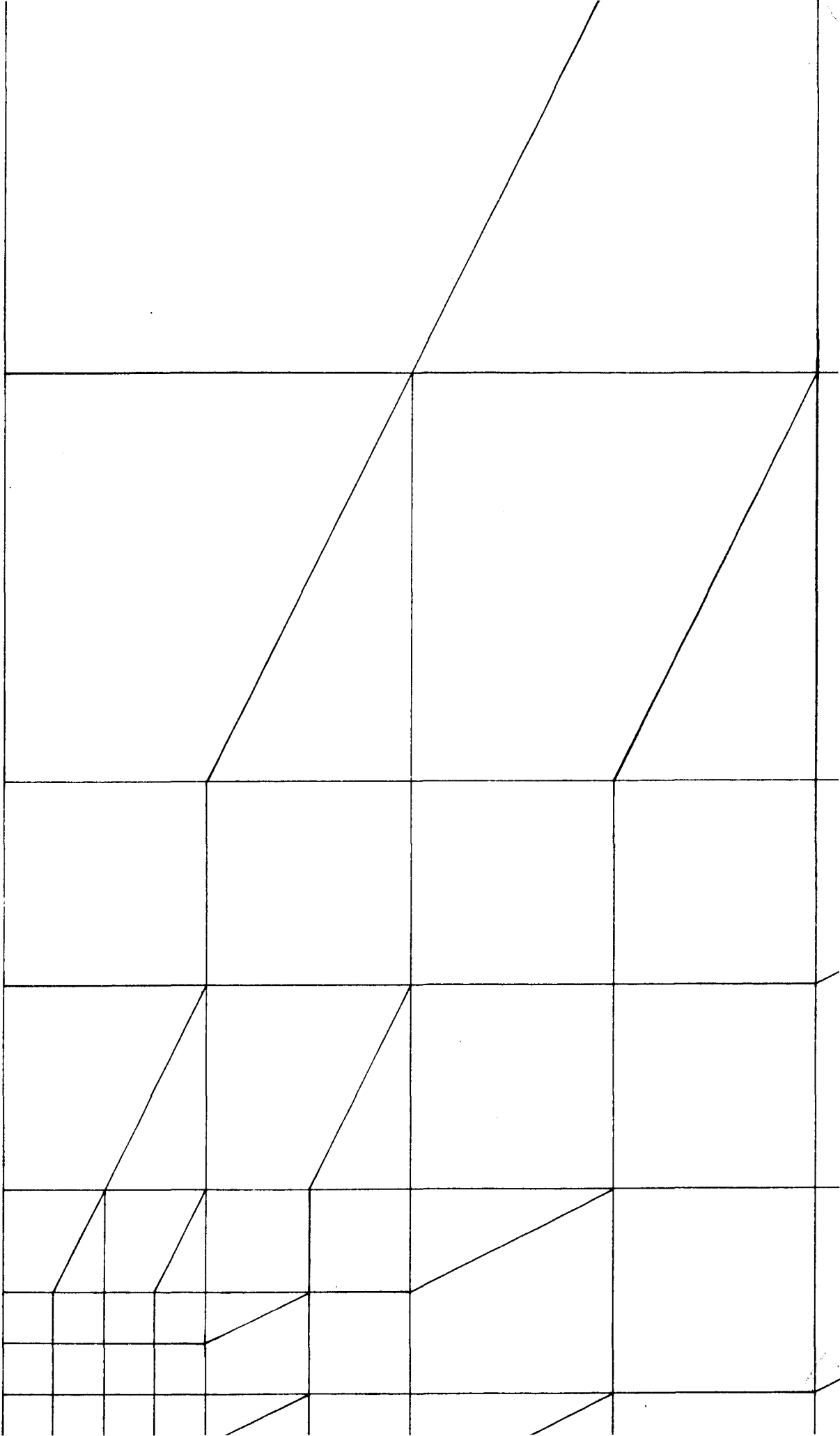
160

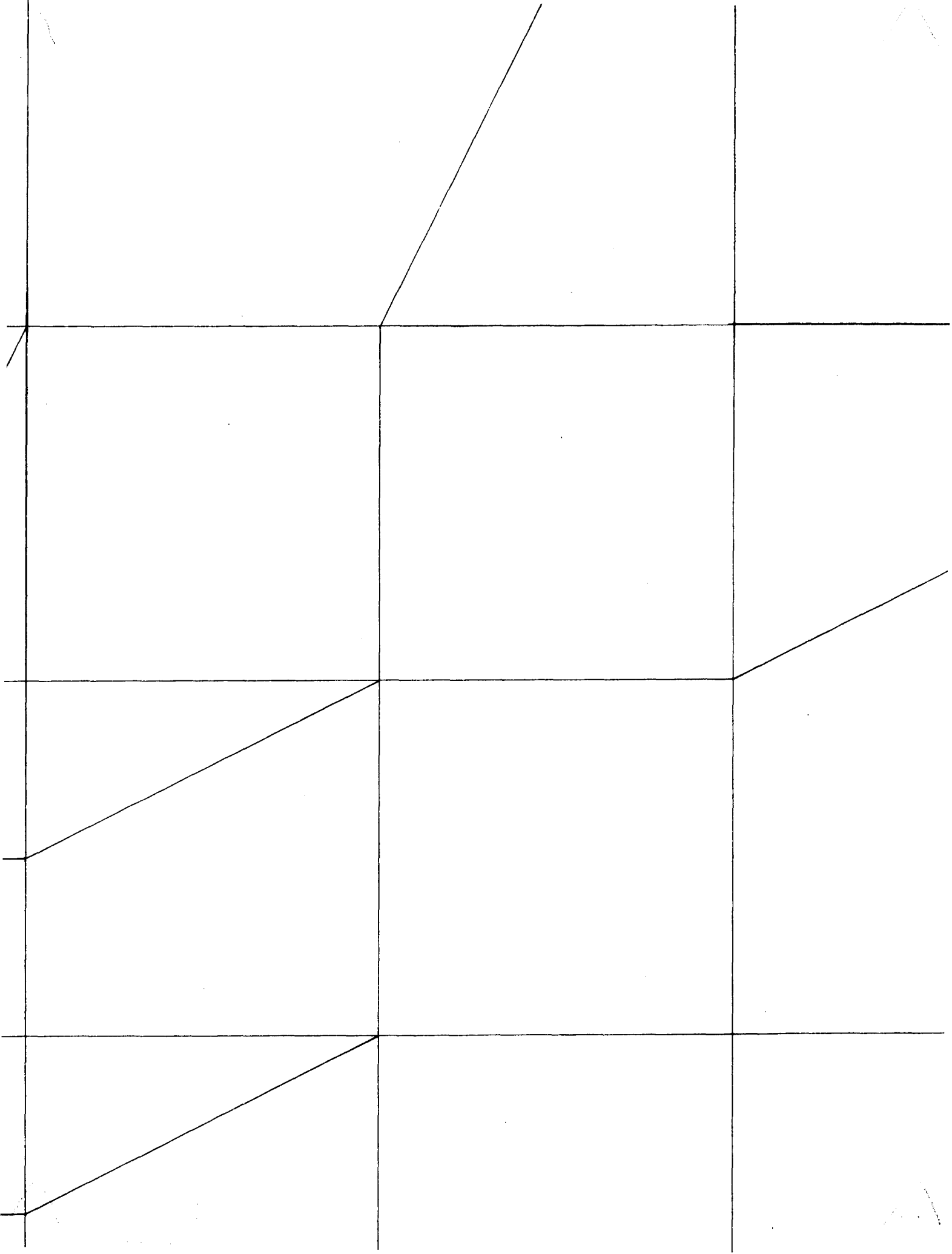
128

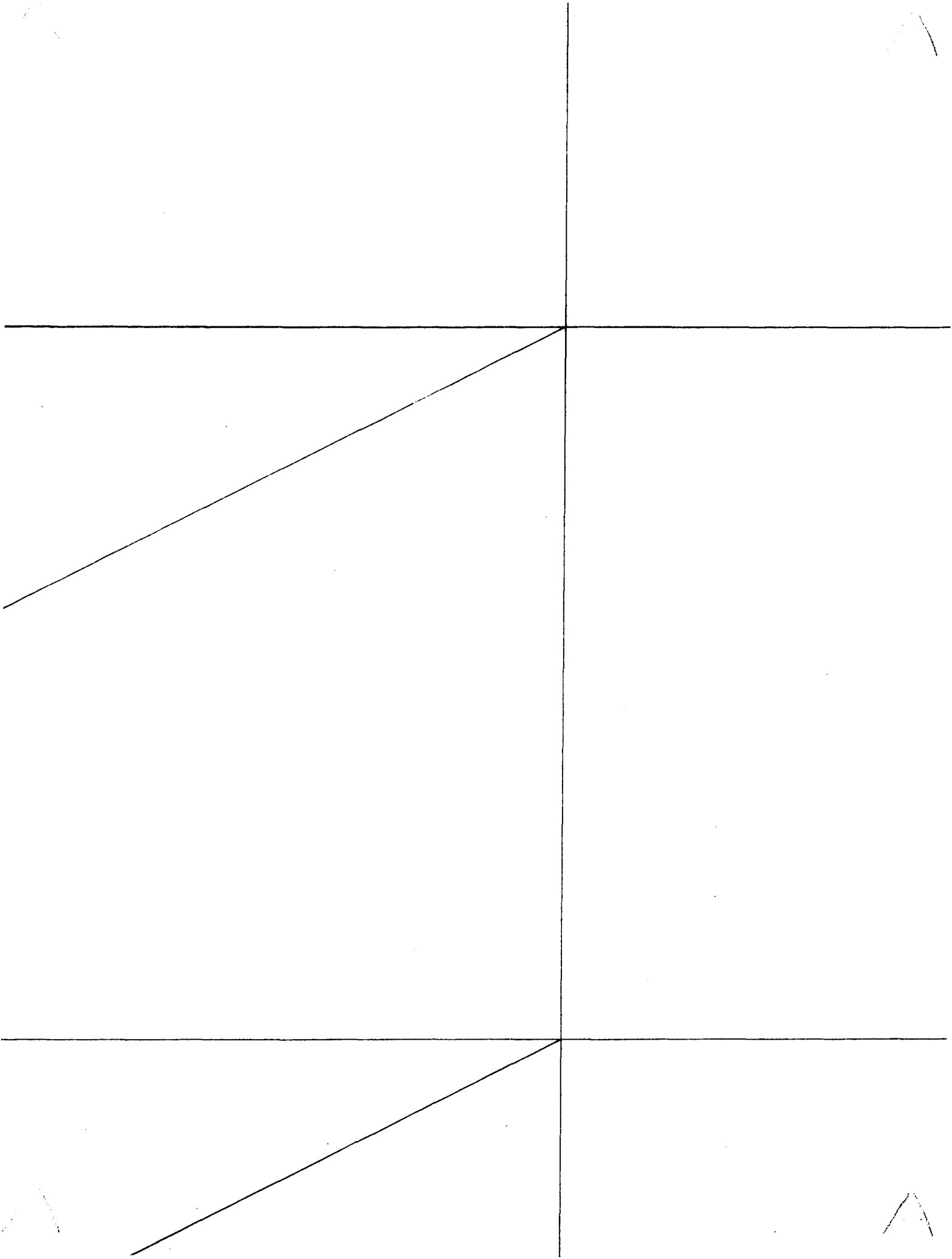
112

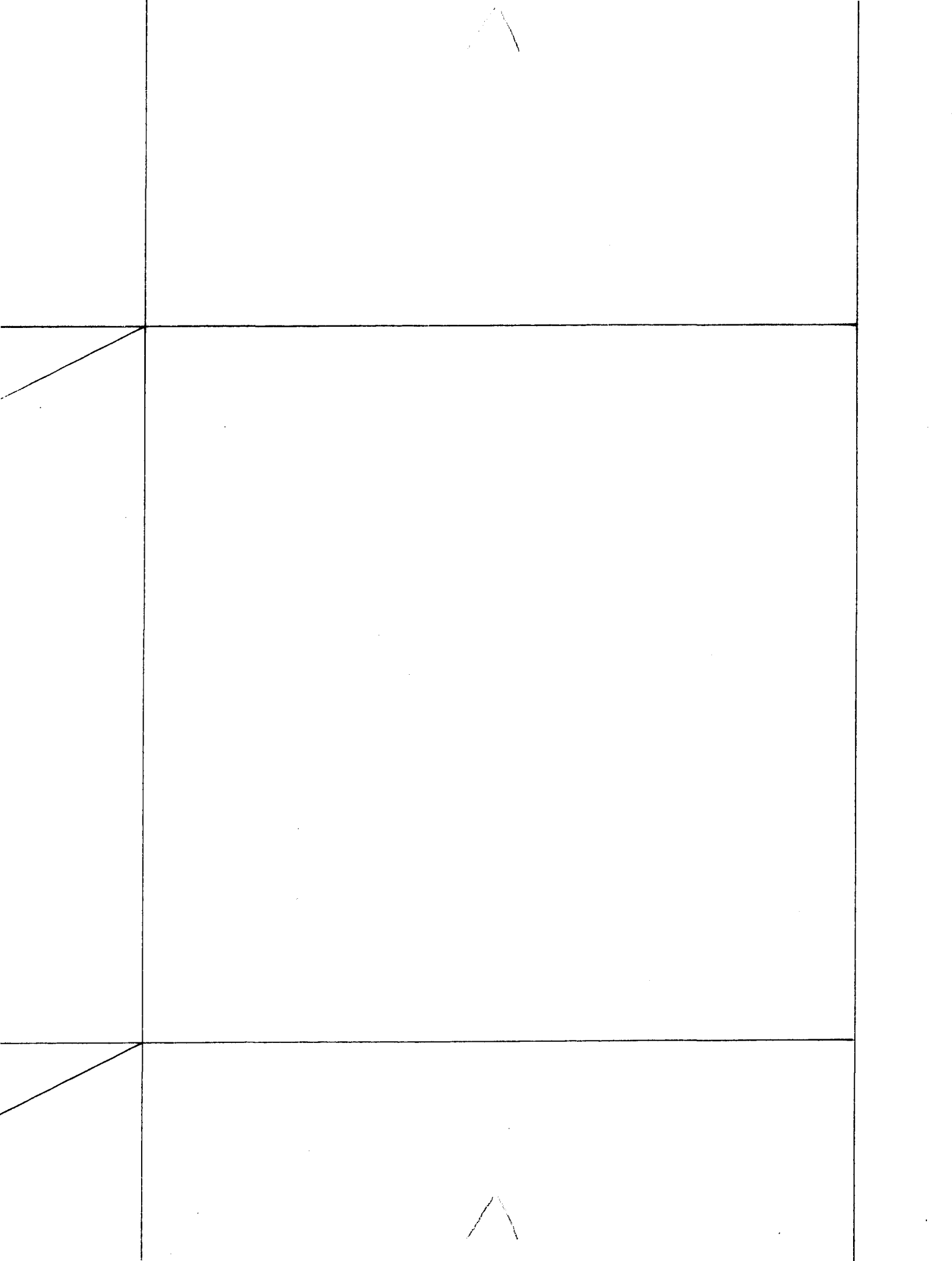
104

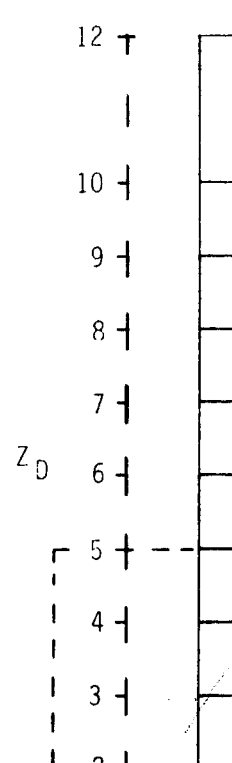
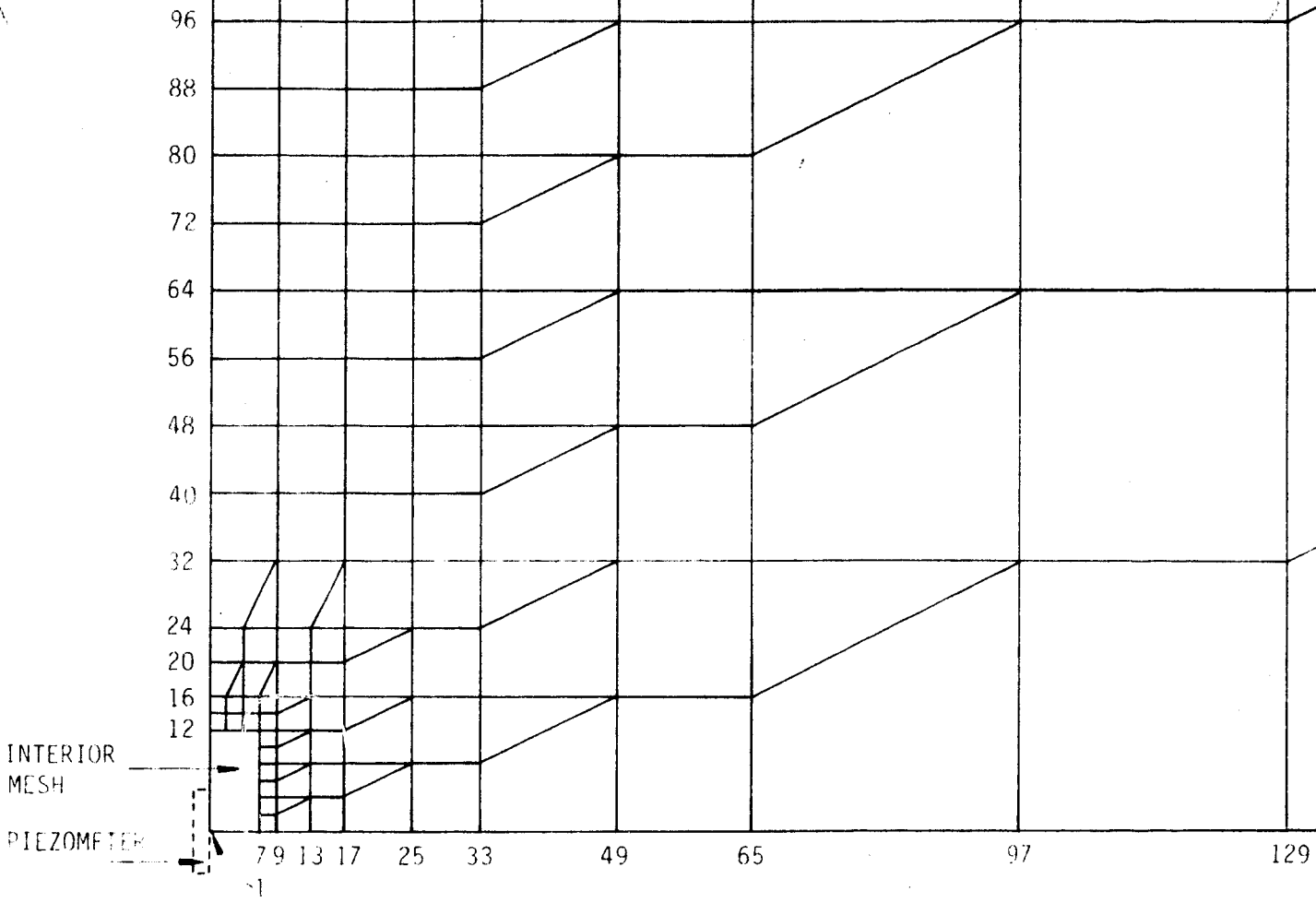
96

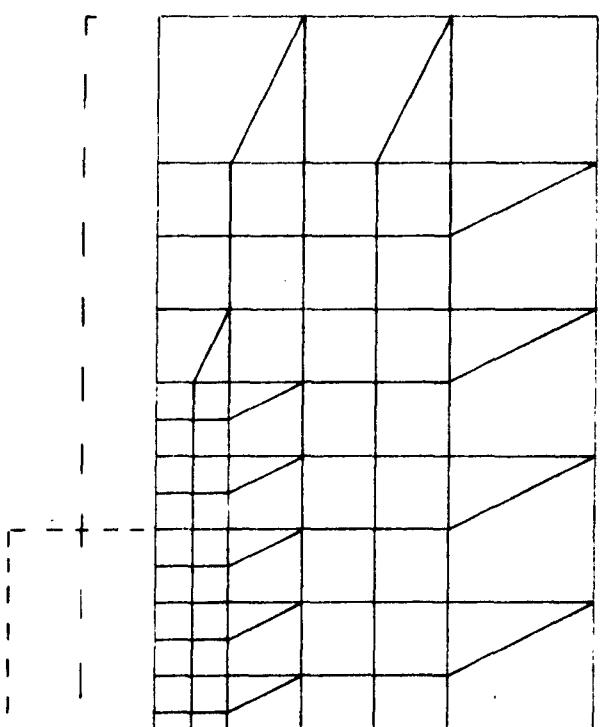
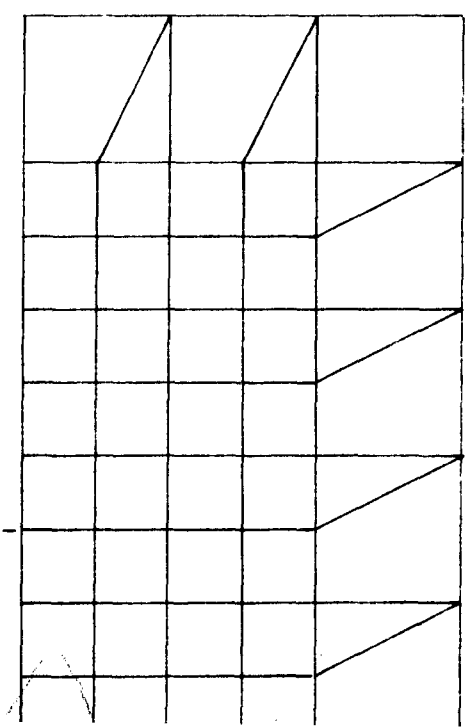
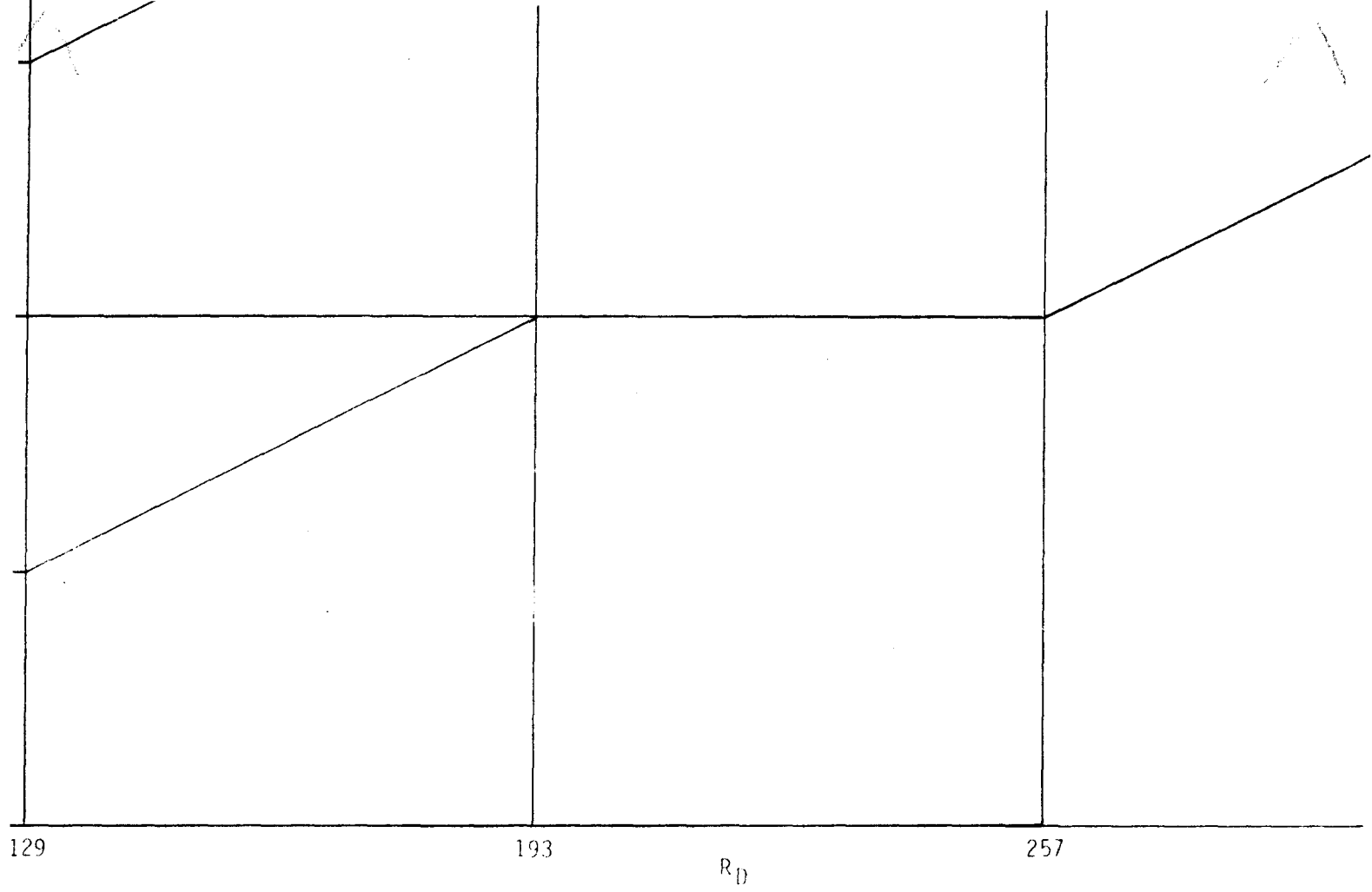


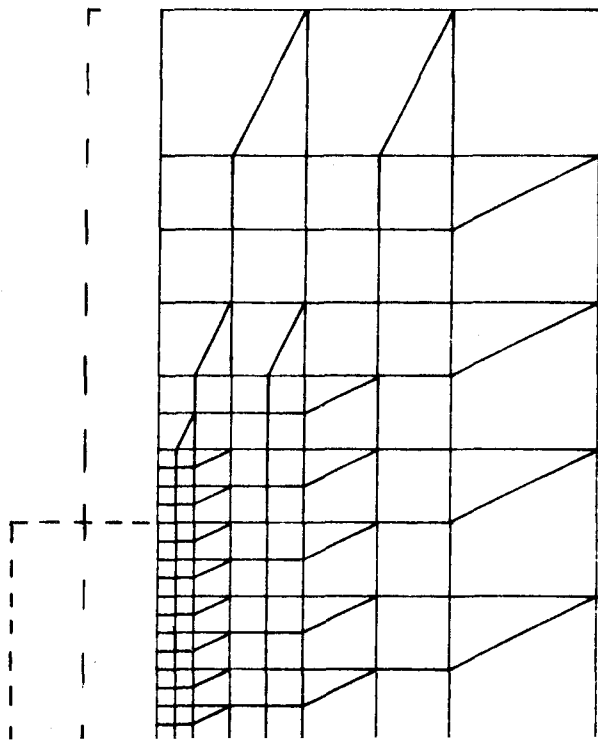








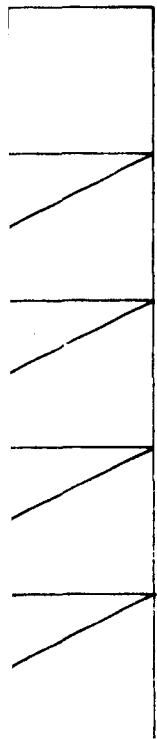






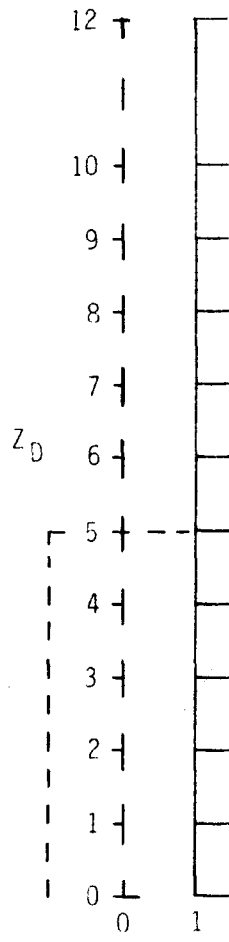
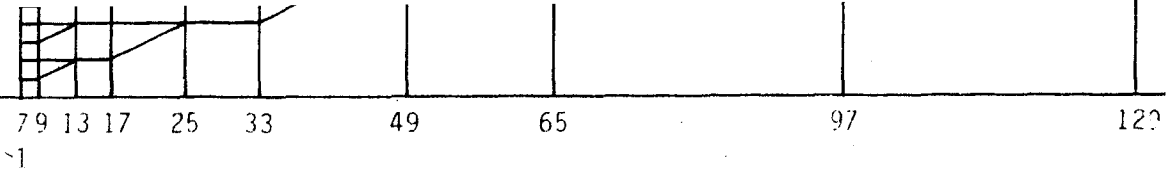
385

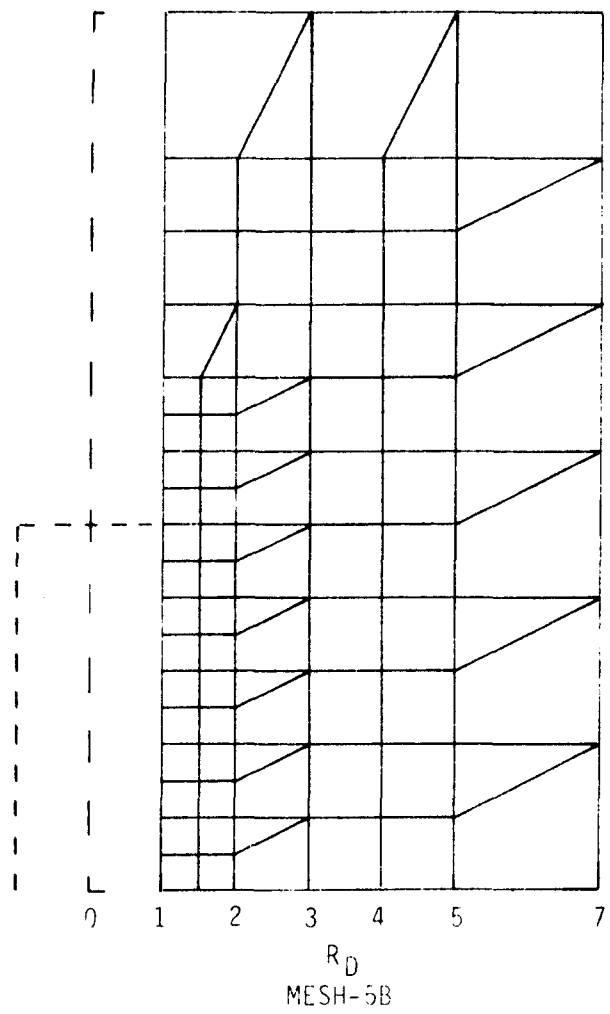
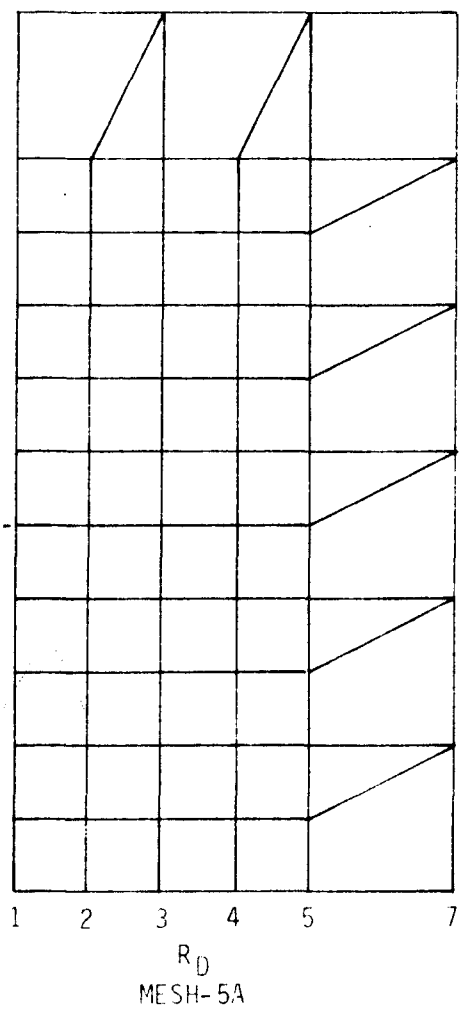
513



INTERIOR
MESH

PIEZOMETER

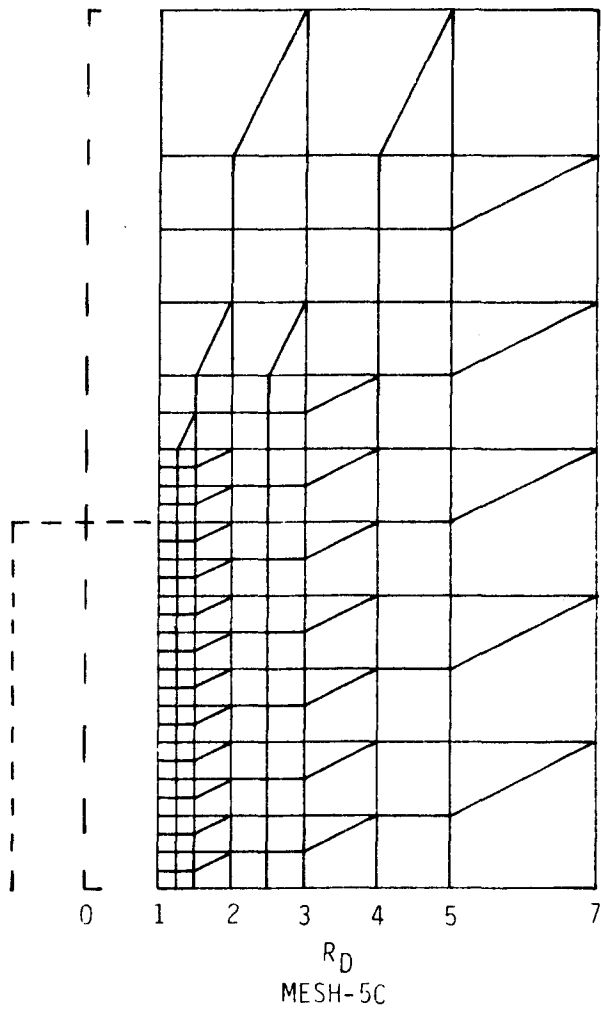




INTERIOR MESHES

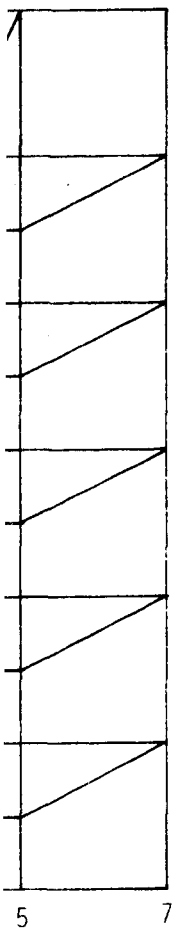
PLATE 2. EXTERIOR MESH AND INTERIOR MESHES FOR NONHORIZONTAL

(F. Marinelli, M.S. Thesis, Department of Hydrology and Water Resour

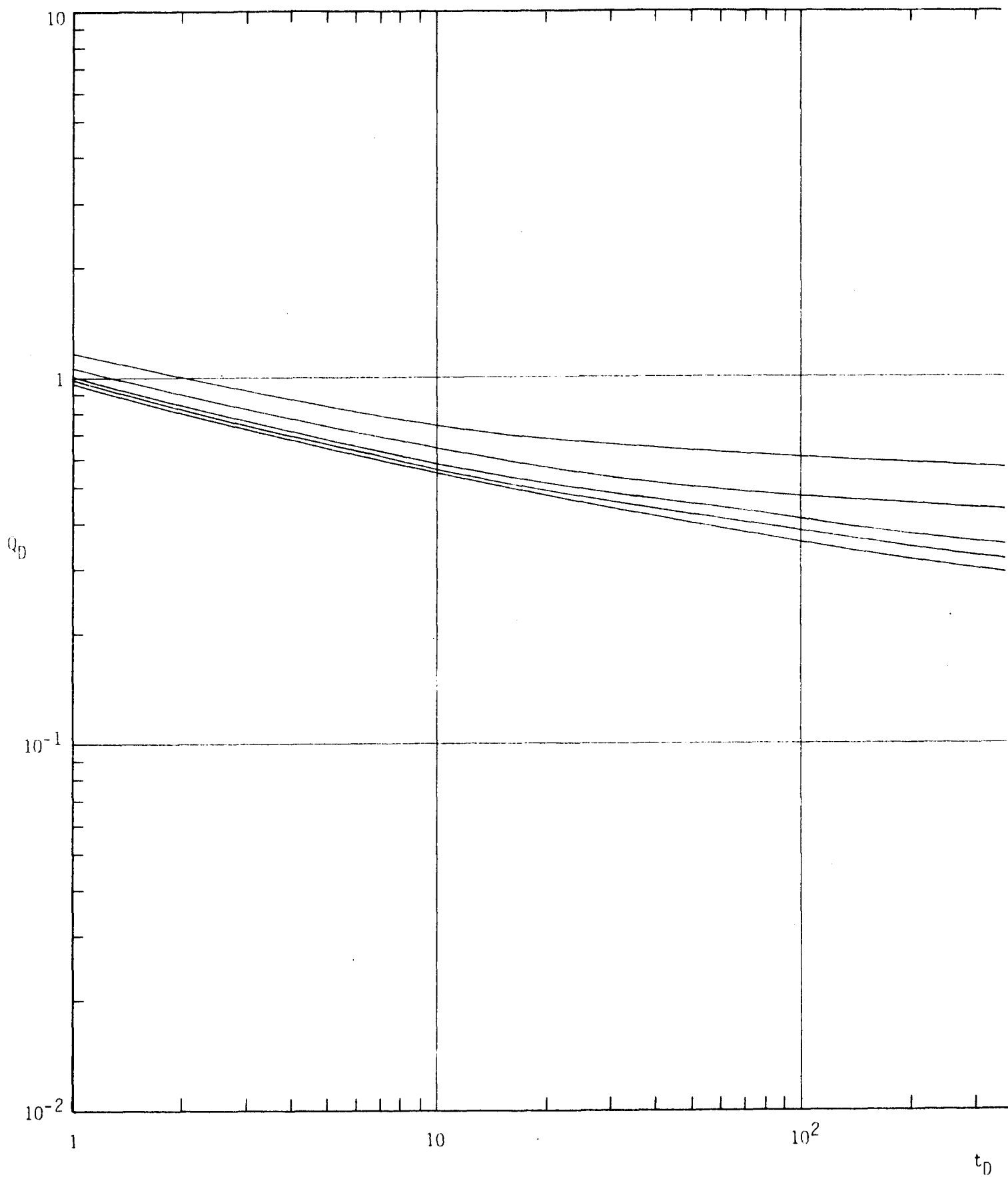


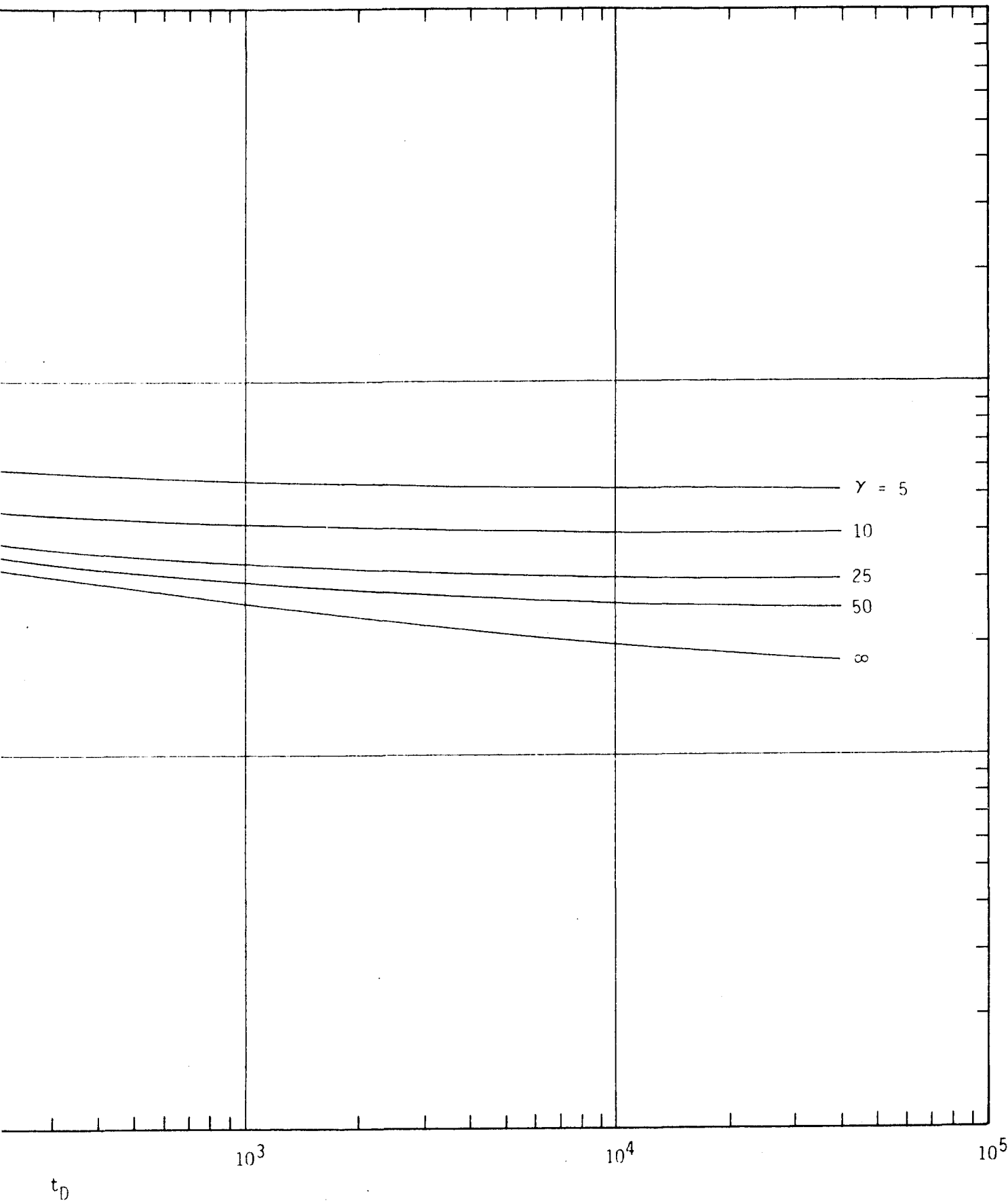
HORIZONTAL FLOW ($\gamma=5$)

Resources, University of Arizona, 1984)



4)





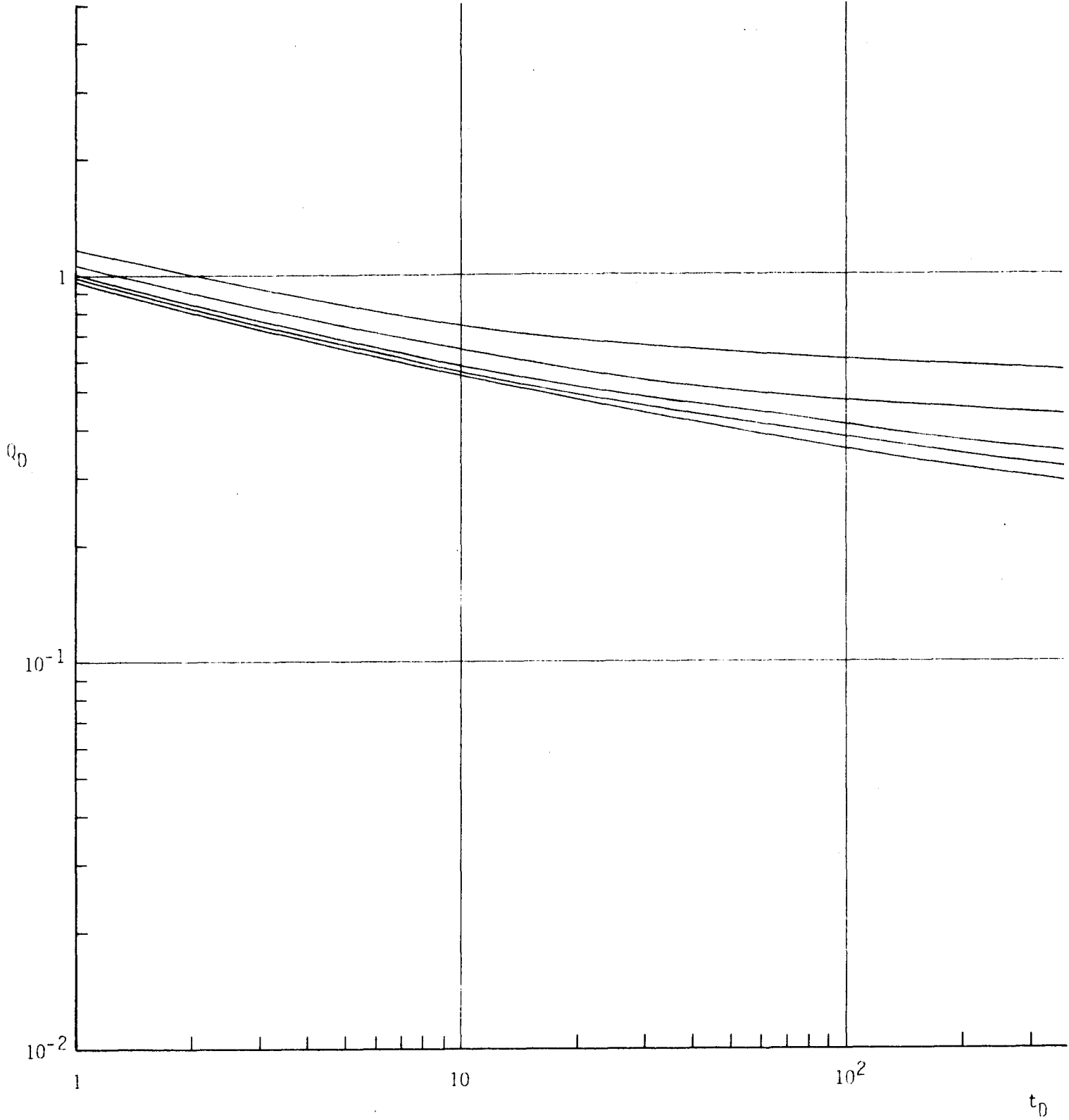
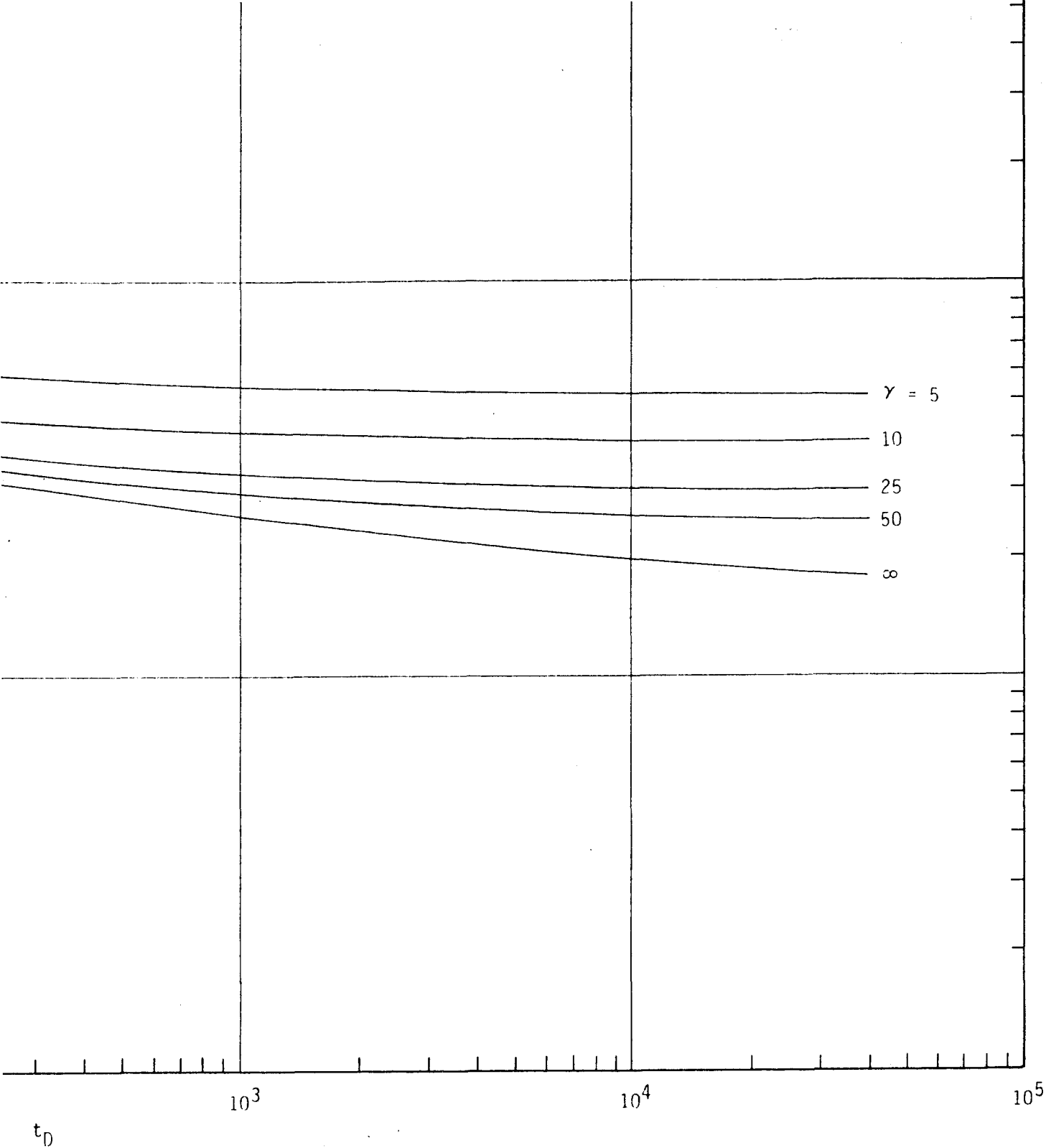


PLATE 3. FULL SIZE TYPE CURVES (Q_D vs. t_D) FOR TR

(F. Marinelli, M.S. Thesis, Department of Hydrolog



OR TRANSIENT NONHORIZONTAL FLOW

hydrology and Water Resources, University of Arizona, 1984)